MOUNTAIN-PLAINS CONSORTIUM

MPC 17-321 | C. Pantelides, D. Brown, J. Parks, and M.J. Ameli

Seismic Retrofit of Spliced Sleeve Connections for Precast Bridge Piers

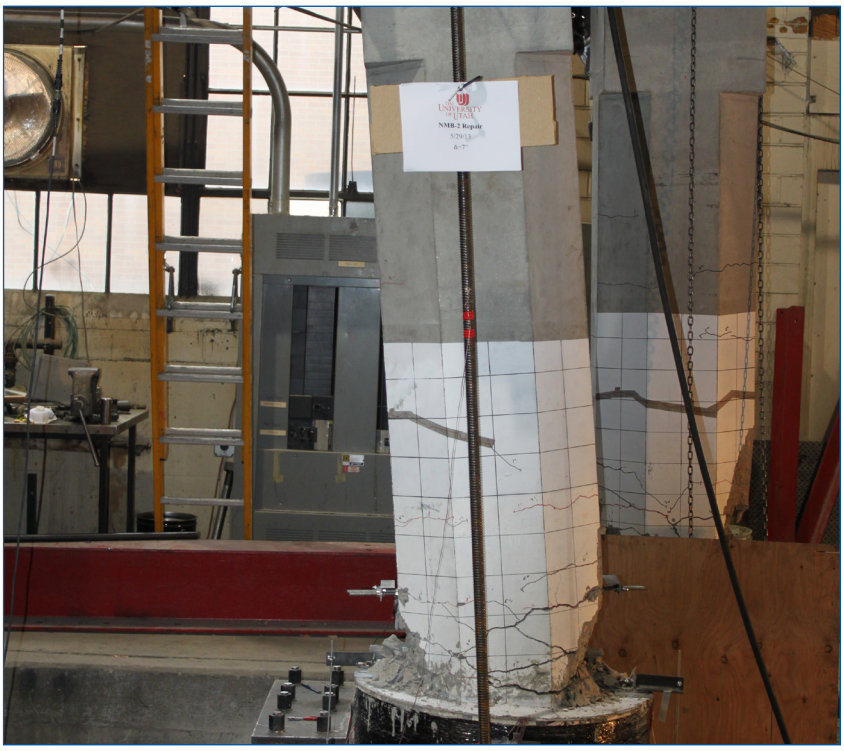

MOUNTAIN-PLAINS CONSORTIUM REGION 8

A University Transportation Center sponsored by the U.S. Department of Transportation serving the Mountain-Plains Region. Consortium members:

Colorado State University
North Dakota State University
South Dakota State University
University of Colorado Denver
University of Denver
University of Utah
Utah State University
University of Wyoming

Seismic Retrofit of Spliced Sleeve Connections for Precast Bridge Piers

Chris P. Pantelides
Professor
Department of Civil and Environmental Engineering
University of Utah
Salt Lake City, Utah, 84112
Phone: (801) 585-3991
Email: c.pantelides@utah.edu

Dylan N. Brown
Graduate Student
Department of Civil and Environmental Engineering
University of Utah
Salt Lake City, Utah, 84112
Phone: (801) 585-3991
Email: dylan.n.brown@utah.edu

Joel E. Parks
Graduate Student
Department of Civil and Environmental Engineering
University of Utah
Salt Lake City, Utah, 84112
Phone: (801) 585-3991
Email: joel.parks@utah.edu

M.J. Ameli
Graduate Student
Department of Civil and Environmental Engineering
University of Utah
Salt Lake City, Utah, 84112
Phone: (801) 585-3991
Email: m.ameli@utah.edu

March 2017

Acknowledgements

The authors acknowledge the financial support provided by the Mountain Plain Consortium (MPC) under project MPC-405, the Utah Department of Transportation, the New York State Department of Transportation, and the Texas Department of Transportation through the Pooled Fund Study Program.

The authors acknowledge Carmen Swanwick and Joshua Sletten, who served on UDOT's Technical Advisory Committee for helping to guide the research. In addition, they appreciate the advice of Harry White, New York State Department of Transportation.

The authors would also like to acknowledge the assistance of Mark Bryant, Zant Doty, Trevor Nye, and Wade Stinson of the University of Utah for their assistance in the experiments.

The following companies made in-kind donations for this project and the authors are grateful to them: Splice Sleeve North America, Inc., ERICO, Sika USA, and Hanson Structural Precast.

Disclaimer

ABSTRACT

Grouted Splice Sleeve (GSS) connectors are being considered for connecting bridge columns, footings, and pier caps in Accelerated Bridge Construction (ABC). A repair technique for precast reinforced concrete bridge column-to-footing and column-to-pier cap joints constructed with GSS connectors has been developed. The repair utilizes prefabricated carbon fiber-reinforced polymer (CFRP) shells, epoxy anchored headed mild steel rebar, and non-shrink concrete to relocate the column plastic hinge. Prior to the repair, undamaged column-to-footing and column-to-pier cap joints constructed with GSS connectors were tested to failure under a quasi-static cyclic lateral load. The as-built column plastic hinge region was subsequently repaired, and the repaired joints were tested following the same cyclic loading protocol as the as-built specimens. The plastic hinge was successfully relocated to the column section adjacent to the repair. The repair method is simple and rapid and could be used to repair bridges constructed with joints utilizing GSS connectors. The method is general and it shows promise for retrofitting or repairing bridges constructed with conventional cast-in-place joints as well.

TABLE OF CONTENTS

EXECUTIVE SUMMARY **1**

1. INTRODUCTION **1**

1.1 Previous Research 1

1. 2 Research Objectives 2

1.3 Outline of Report 5

2. DETAILS OF AS-BUILT JOINTS AND TEST SETUP **6**

2.1 As-built Joint Details 6

2.2 Test Setup 10

2.3 Loading Protocol 11

3. EXPERIMENTAL RESULTS FOR AS-BUILT JOINTS **13**

3.1 As-Built Column-to-footing Joint NM-O 13

3.2 As-built Column-to-pier cap Joint LE-O 14

4. DESIGN OF THE REPAIR AND EXPERIMENTAL RESULTS **16**

4.1 Repair Design 16

4.2 Repair Procedure 20

4.3 Experimental Results of Repaired Joints 24

4.3.1 Repaired Column-to-footing Joint NM-R 24

4.3.2 Repaired Column-to-pier cap Joint LE-R – Static Pushover 35

4.3.3 Repaired Column-to-pier cap Joint LE-R – Cyclic Test 39

4.3.4 Comparative Study of As-Built and Repaired Joints 43

5. CONCLUSIONS **44**

5.1 Summary 44

5.2 Findings 44

6. REFERENCES **45**

LIST OF TABLES

Table 1.1 Test matrix 4

Table 2.1 As-built and repair material properties 10

Table 4.1 Repair concrete mix design for NM-R and LE-R 19

Table 4.2 Comparison of test results 43

LIST OF FIGURES

Figure 1.1 Idealized bridge pier subjected to double curvature showing tested subassemblies 3

Figure 1.2 Two types of GSS incorporated in this research: (a) FGSS connector; (b) GGSS connector 3

Figure 1.3 FGSS vs GGSS connections 4

Figure 1.4 Configuration of test specimens 5

Figure 2.1 Prototype bridge with highlighted portions representing specimen design 7

Figure 2.2 Precast column-to-footing specimen NM-O prior to grouting: (a) column, (b) footing 8

Figure 2.3 General design and detailing of joint region for specimen NM-O 8

Figure 2.4 Rebar cages for specimen NM-O: (a) column, (b) footing 9

Figure 2.5. Reinforcement details for specimen LE-O 9

Figure 2.6 Test setup 11

Figure 2.7 Applied lateral displacement history 12

Figure 3.1 NM-O hysteresis curve 13

Figure 3.2 Final damage of specimen NM-O: (a) ultimate displacement of 7 inches, (b) column and footing cracking, (c) plastic hinge region, (d) fractured east longitudinal rebar 14

Figure 3.3 Hysteresis response of specimen LE-O 15

Figure 3.4 Final damage of specimen LE-O showing plastic hinge region 15

Figure 4.1 Graphical representation of design loads for simplified design procedure 16

Figure 4.2 Repair design details for specimen NM-O 18

Figure 4.3 CFRP composite preparation: (a) saturation, (b) making shells, (c) split prefabricated shells, (d) wet layup 21

Figure 4.4 Headed rebar installation: (a) core drilling, (b) epoxy injection, (c) inserting rebar, (d) after installation 22

Figure 4.5 Repair concrete: (a) before casting, (b) vibrating, (c) finishing concrete after casting, (d) wooden formwork and weights 23

Figure 4.6 Split CFRP shell for specimen LE-R 23

Figure 4.7 Specimens displaced to the east at the maximum displacement: (a) NM-O, (b) NM-R 24

Figure 4.8 NM-R repaired specimen hysteresis curve 25

Figure 4.9 NM-R repaired specimen backbone curve 25

Figure 4.10 Transverse CFRP crack at white line 3 inches below top of CFR shell 26

Figure 4.11 NM-R repaired specimen curvature profile up to 4-in. displacement step 27

Figure 4.12 NM-R test through the 6-in. displacement step: (a) radial cracks after 1-in. displacement step, (b) first crack during 2-in. displacement step, (c) gapping at repair-column interface during the 6-in. displacement step, (d) shear x-crack after the 4-in. displacement step 28

Figure 4.13 NM-R test through final damage state: (a) major spalling during 5-in. displacement step, (b) damage level after 6-in. displacement step, (c) damage state during 7-in. displacement step, (d) final damage state 29

Figure 4-14 NM-R CFRP wrap strain gauge data averaged by height 30

Figure 4.15 NM-R CFRP wrap strain gauge data from top 3-in. band: (a) East, (b) West 31

Figure 4.16 NM-R west face wrap strain profile up to 4-in. displacement step 32

Figure 4.17 NM-R headed bar strain gauge data from 7.5 inches above the footing level 33

Figure 4.18 Comparison of hysteresis curves for NM-O and NM-R 33

Figure 4.19 NM-R performance comparison: (a) hysteretic energy dissipation, (b) normalized stiffness 34

Figure 4.20 Specimen LE-R monotonic pushover at maximum drift 36

Figure 4.21 Specimen LE-R monotonic pushover damage 36

Figure 4.22 LE-R monotonic pushover curve 37

Figure 4.23 LE-R monotonic pushover moment-curvature 38

Figure 4.24 LE-R east CFRP jacket hoop strains 38

Figure 4.25 LE-R headed bar strains 39

Figure 4.26 Test Comparison: (a) LE-O at maximum drift, (b) LE-R at maximum drift 40

Figure 4.27 Final damage of repaired specimen LE-R: (a) west face, (b) east face 40

Figure 4.28 Repaired specimen LE-R hysteresis curve 41

Figure 4.29 LE-R transverse CFRP crack 42

Figure 4.30 Comparison of test results for as-built specimen LE-O and repaired specimen LE-R 43

LIST OF ACRONYMS

AASHTO	American Association of State Highway and Transportation Officials
ACI	American Concrete Institute
CFRP	Carbon Fiber Reinforced Polymer
GSS	Grouted Splice Sleeve
MPC	Mountain-Plains Consortium
PBES	Prefabricated Bridge Elements and Systems
SDC	Seismic Design Category
SDC	Seismic Design Criteria
UDOT	Utah Department of Transportation

EXECUTIVE SUMMARY

Prefabrication of bridge structural components is a highly effective method and is one of the Accelerated Bridge Construction (ABC) methods under the category of Prefabricated Bridge Elements and Systems (PBES) promoted by the Federal Highway Administration. The joints or connections between a precast concrete column and pier cap and between a column and footing play an important role in the overall seismic performance of a bridge. This report describes a research study developed to investigate the retrofit of joints for ABC components of bridges located in high-seismic regions. Grouted Splice Sleeve (GSS) connectors were used to construct column-to-footing and column-to-pier cap joints. Half-scale test models were designed and constructed based on typical reinforced concrete bridges in the state of Utah. Cyclic quasi-static loading was applied to a column-to-footing specimen and a column-to-pier cap half-scale test specimen. The precast column-to-footing joint incorporated one type of GSS where the bars were grouted at both ends (GGSS); the precast column-to-pier cap joint used a different GSS type where one bar was threaded into one end and the other bar was grouted into the opposite end (FGSS). After the as-built test, the GGSS column-to-footing joint was repaired and tested again. Similarly, the FGSS column-to-pier cap joint was repaired and tested again. The repair utilized prefabricated carbon fiber-reinforced polymer (CFRP) shells, epoxy anchored headed mild steel rebar, and non-shrink concrete to relocate the column plastic hinge. Experimental results show that performance of the repaired precast test specimens was satisfactory. The plastic hinge was successfully relocated to the column section adjacent to the repair. The method is simple and rapid and could be used to repair bridges constructed with joints utilizing GSS connectors. The report compares the performance of the precast joints to the repaired joints utilizing both GGSS and FGSS connectors. The method successfully restored the performance of the damaged specimens in terms of displacement capacity, load capacity, energy dissipation, and stiffness.

1. INTRODUCTION

Accelerated Bridge Construction (ABC) refers to a bridge construction type that incorporates innovative techniques, methodologies, and materials to efficiently reduce construction time and traffic disruption. It also provides a higher level of work-zone safety for workers and commuters, and improves environmental-friendly activities. Prefabrication of bridge structural components is a highly effective method in this process and is one of the ABC methods under the category of Prefabricated Bridge Elements and Systems (PBES) promoted by the Federal Highway Administration. Many bridges have been built following ABC standards. Local examples include the I-15 CORE Provo Center Street Interchange, the Riverdale Road over I-84 Bridge, and the I-15 South Layton Interchange.

Grouted splice sleeves (GSS) are gaining attention as a method for connecting precast concrete bridge elements using ABC standards. The use of GSS connectors to connect bridge elements in areas of high seismicity is currently being studied [1-3]. Recent projects, including construction of rail train bridges for the Frontrunner light rail in Salt Lake City, show promise for GSS connectors becoming a popular precast concrete connection option in areas of moderate-to-high seismicity. The expected increase in use of GSS connectors for joining bridge elements poses the need for a post-earthquake repair technique, which is the focus of the research.

Current capacity-based bridge design procedures direct damage of bridge assemblies to columns, thereby protecting footings and pier caps; thus, the repair method has been developed to improve the seismic performance of column plastic hinges. The repair method developed in this project uses carbon fiber-reinforced polymer (CFRP) shells, headed mild steel rebar, and non-shrink concrete to strengthen the column plastic hinge region, relocating subsequent damage to the area of the column adjacent to the repaired section. This plastic hinge relocation is achieved by increasing the column cross-section of the damaged region of the column. For the half-scale specimens tested in this study, the column was increased from a 21-in. octagonal section to a 30-in. diameter circular section over a column height of 18 inches. The repair method can be implemented rapidly and uses standard construction techniques and a small amount of readily available materials. The purpose of the repair is to restore the load and displacement capacities of an earthquake damaged column, alleviating the need for bridge replacement.

GSS connectors have been used for bridge joints in non-seismic regions in the past. Recently, research programs at the University of Utah [1], University of Nevada at Reno [2], and University of Bergamo [3] have investigated the applicability of GSS connectors for bridge joints in seismic regions. The findings from these research programs are showing acceptable levels of cyclic performance. However, the precast specimens do not quite match the performance of their monolithic counterparts in terms of displacement ductility and energy dissipation. The specimens referred to as “as-built” specimens in this research are precast concrete column-to-footing and column-to-pier cap joints with GSS connectors being studied at the University of Utah [1].

1.1 Previous Research

Extensive research has been conducted for retrofit and repair of bridge columns utilizing CFRP composites [4, 5], steel [6], and concrete jacketing [7]. The objective of these studies was to increase the flexural performance of the column plastic hinge region through jacketing. Recently, a precast concrete joint constructed with GSS connectors was repaired after being tested [3]. The repair consisted of a grout jacket made from high-strength shrinkage-compensating grout. The exact details of the retrofit are not known, but the results were unsatisfactory in terms of displacement ductility and energy dissipation capacity.

Little research has been conducted that investigates plastic hinge relocation as a method to control the location of damage or to restore the diminished load and displacement capacity of earthquake-damaged bridge columns. Hose et al. [8] studied the effectiveness of strengthening likely plastic hinge regions to force damage away from joint regions. The plastic hinge regions were successfully relocated by increasing the longitudinal and transverse reinforcement ratios in the traditional plastic hinge regions. Lehman et al. [7] studied multiple concrete jacketing techniques, including techniques to relocate the original plastic hinge for columns of varying damage states. One repair, performed on a column with fractured longitudinal bars, increased the original column cross-section from a 24-in. to a 30-in. diameter over a column length of 22 inches. The increased cross-section was reinforced with double headed rebar in the longitudinal direction and a spiral at a 1.5-in. pitch in the transverse direction. The intent of the repair was to relocate the plastic hinge region to the top of the repaired section. The repair was successful but did not restore the diminished displacement capacity of the specimen. Recently, Rutledge et al. [9] used CFRP composites oriented in the longitudinal and transverse direction to perform plastic hinge relocation for earthquake-damaged monolithic column-to-footing specimens. The damage state of the specimens prior to the repair was severe, including longitudinal bars that had buckled or fractured. Three tests were performed on the repaired specimens; plastic hinge relocation was achieved for specimens which had buckled bars. However, the repair proved incapable of restoring the diminished load and displacement capacities if the longitudinal bars had fractured prior to the repair.

1.2 Research Objectives

This report describes the development of a repair method for earthquake-damaged modern ABC column-to-footing and column-to-pier cap joints connected using GSS connectors. In order to design and test the repaired joints, as-built specimens were severely damaged, and the damage state was assessed. Tests were performed on an undamaged precast column-to-footing and a column-to-pier cap joint connected using GSS connectors, referred to as the as-built specimens. After testing and assessing the performance of the as-built specimens, a repair design and repair procedure were developed and implemented for both types of damaged specimens. The repaired assemblies were then retested following the same procedures as the as-built specimens. After the completion of the repair for the as-built specimens, the assemblies are referred to as the repaired specimens.

The column-to-footing and column-to-pier cap joints were tested in single curvature, replicating an idealized subsection of a multicolumn bridge subassembly that is subjected to double curvature. The bridge subsections being tested are the column-to-footing and column-to-pier cap portions of the bridge subassembly from the point of inflection down or up, as shown in Figure 1.1. The specimens were designed to be half-scale models of typical bridges in Utah. All the as-built and repaired specimens were tested laterally with a constant axial load of 6% of the column's 28-day concrete strength axial load capacity, representing typical axial loading of bridge structures. The lateral load was applied following a displacement controlled quasi-static cyclic loading protocol, which remained the same for all tests.

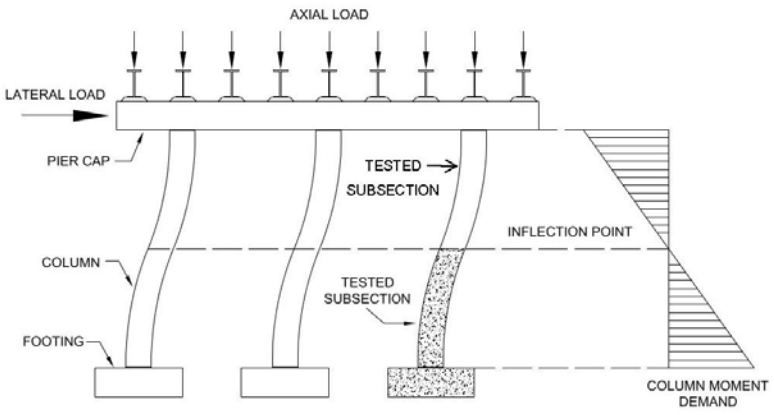

Figure 1.1 Idealized bridge pier subjected to double curvature showing tested subassemblies

Grouted Splice Sleeves (GSSs), alternatively called mechanical rebar splices or grout-filled steel sleeves, are hollow steel cylinders made of ductile iron. Figure 1.2 shows two types of GSSs utilized in this research project. Steel bars from two reinforced concrete components that are to be connected to each other are grouted at both sleeve ends for the longer GSS (NMB 8U-X), or threaded into one end and grouted at the opposite end in the short GSS (LK8). Figure 1.3 shows the shorter GSS, referred to as FGSS, in which the threaded factory dowel is fastened to one end while the field dowel is grouted in the other end of the sleeve. This GSS is a product of Erico®, commercially available under Lenton® Interlok.

The longer alternative is referred to as GGSS, indicating that rebar is grouted at both ends of the sleeve, and is also shown in Figure 1.3. This GSS is a product of Splice Sleeve North America and commercially available under the name of NMB Splice-Sleeve®. The original research was geared toward conducting reversed cyclic tests on half-scale specimens connected by two different GSSs, to investigate their seismic performance in comparison to conventional cast-in-place bridge construction. Complete details of the original research for joints with FGSS and GGSS connectors can be found in the MPC-392 report (Pantelides et al. [9]).

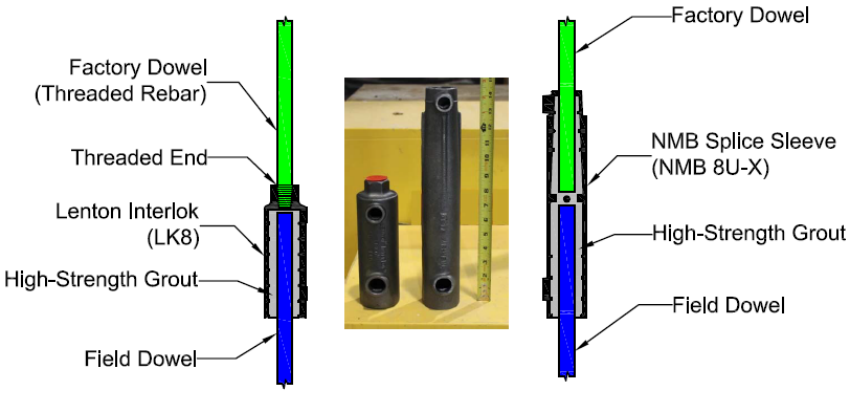

Figure 1.2 Two types of GSS incorporated in this research: (a) FGSS connector; (b) GGSS connector

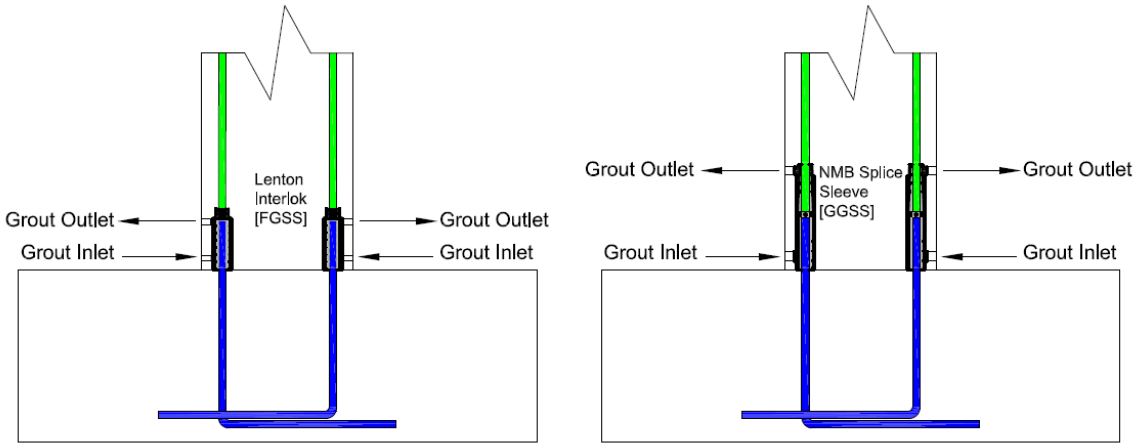

Figure 1.3 FGSS vs. GGSS connections

The present report describes a research program conducted to develop a repair method for earthquake-damaged modern ABC column-to-footing and column-to-pier cap joints connected using GSS connectors. In this experimental program, precast reinforced concrete components were built and connected with GGSS connectors to construct a column-to-footing joint (NM-O); in addition, FGSS connectors were used to construct a column-to-pier cap joint (LE-O). Both of these specimens were then repaired with the method developed in this research and were re-tested; specimen NM-O was repaired and retested as specimen NM-R, and specimen LE-O was repaired and re-tested as specimen LE-R. The test matrix is shown in Table 1.1. Figure 1.4 presents the configuration of the tested specimens. For specimen NM-O, the GGSS connectors were placed in the footing; and for specimen LE-O, the FGSS connectors were in the pier cap. A pre-grout installation technique was adopted to facilitate the erection process, which is diferent than the grouting operation indicated in Figure 1.3.

Table 1.1 Test matrix

Specimen	**Designation**	**Sleeve**	**Sleeve**
		Type	**Location**
NM-O	Original	NMB-8UX	Footing
LE-O	Original	LK-8	Pier Cap
NM-R	Repaired	NMB-8UX	Footing
LE-R	Repaired	LK-8	Pier Cap

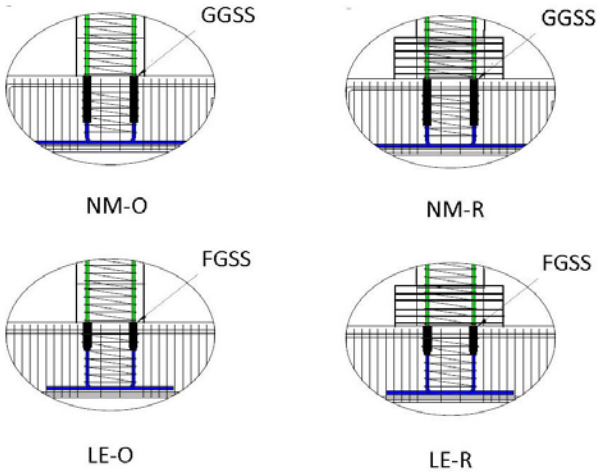

Figure 1.4 Configuration of test specimens

In the grouting process used for NM-O and LE-O, plastic plugs were used to seal the GGSS and FGSS connector inlet and outlet, before casting concrete. During the installation, all GGSS connectors were first filled with grout from the wide end opening. A Kenrich GP-2HD hand pump was utilized to pump the grout into the GGSS connectors by inserting the nozzle into the wide end opening.

The main objective of conducting this research was to gain more knowledge about GSS connectors and their properties, understand their seismic performance, and develop a repair method for earthquake-damaged modern ABC column-to-footing and column-to-pier cap joints connected using GSS connectors.

1.3 Outline of Report

This report describes the sequence of tasks accomplished for carrying out the research. Section 1 provides the background and previous research on precast bridge joints and the research objectives. Section 2 provides the details of the as-built precast bridge joint specimens, the test setup, and loading protocol. Section 3 is focused on the experimental results for the as-built column-to-footing and column-to pier cap joints. The repair design, repair procedure, and experimental results of the column-to-footing and column-to-pier cap repaired joints are presented in Section 4. Section 5 includes the summary of the report together with the most significant findings.

2. DETAILS OF AS-BUILT JOINTS AND TEST SETUP

2.1 As-built Joint Details

The specimens were designed and detailed to simulate typical prototype bridges constructed in the state of Utah, following the AASHTO LRFD Bridge Design Specifications [10], and the AASHTO Guide Specifications for LRFD Seismic Bridge Design [11], in accordance with capacity-based design procedures. A circular configuration of column longitudinal bars and an octagonal column cross-section were adopted to facilitate the process of precasting the columns, since this is the method of choice in Utah. Currently, the aforementioned design codes in addition to the Caltrans Seismic Design Criteria (SDC) inhibit the splicing of rebar, including mechanical anchorage devices in the plastic hinge region of ductile members for bridges located in moderate-to-high seismic regions [12]. In the AASHTO Guide Specifications for LRFD Seismic Bridge Design [10], this would apply to Seismic Design Categories (SDCs) C and D. Thus, the preliminary design and detailing was developed for specimens without any type of GSS, i.e., cast-in-place specimens for each category. The design was then adjusted to accommodate the GSS within the precast specimens as needed, and essential modifications were considered accordingly.

The test specimens were half-scale models of common prototype highway bridges in Utah. In order to achieve an acceptable test model, many multi-column bent cap systems were studied, including the Riverdale Road Bridge over I-84. The column dimensions, main longitudinal bars and configuration, and footing or cap beam dimensions were obtained by considering approximately 50% of the actual properties. Figure 2.1 depicts a sample prototype bent system in which areas of interest for this research are shown. The column height for all specimens was selected to be 8 feet 6 inches with a 21-in. square column head in the top 1 foot 6 inch portion. The lateral load, however, was intended to be applied at a height of 8 feet from the column end. The cross section changed to an octagon along the remainder of the column height to facilitate casting of concrete.

Both as-built specimens NM-O and LE-O were constructed with precast reinforced concrete elements. NM-O was precast as two separate elements, a column, and a footing, and subsequently connected using GSS connectors. LE-O was precast as two separate elements, a column, and a pier cap, and later connected using GSS connectors.

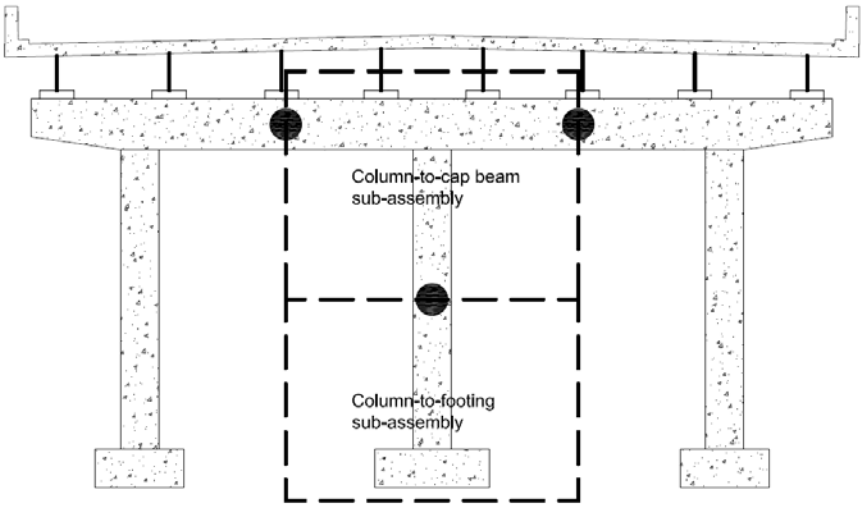

Figure 2.1 Prototype bridge with highlighted portions representing specimen design

Specimen NM-O was connected using GGSS connectors; this type of GSS connection uses grout to secure the rebar at both ends of the connection. The GGSS connectors used were NMB splice sleeves, size 8U-X, as shown in Figure 1.2. Specimen NM-O had the GGSS connectors precast into the footing, as shown in Figure 2.2(b). The GSS connectors are precast into an element with rebar from the connecting element extending into the sleeve. Special care is taken to ensure that the sleeve remains void of concrete during casting. Upon assembly, rebar protruding from the concrete of the element without the GGSS connectors is inserted into the sleeves. The bars that extend from the element cast without the GGSS are referred to as field dowels. Both the field dowels and the bars cast into the GGSS are grouted with a high-strength non-shrink grout to complete the connection.

The column cross-section is non-prismatic with a 21-in. square top section extending 18 inches from the top of the column, changing to a 21-in. octagonal section for the rest of the column length. The square top was designed to easily connect with the lateral load application system. The octagonal column cross-section was used over the length being tested to match the current bridge geometry used by the Utah Department of Transportation. The octagonal cross-section is 7-ft. long and includes the probable plastic hinge region adjacent to the column-footing interface. The footing is 6-ft. long in the direction of the lateral load application, 3-ft. wide and 2-ft. deep. The size of the elements was designed to be approximately half-scale of typical bridge dimensions.

The reinforcement details for specimen NM-O are shown in Figure 2.3The column reinforcement consists of six No.8 longitudinal steel bars and a No. 4 spiral at a pitch of 2.5 inches. The longitudinal and volumetric transverse reinforcement ratios were 1.3% and 1.9%, respectively. The NM-O footing reinforcement consists of 18 No. 8 longitudinal steel bars, a No. 4 spiral, and two overlapping No. 4 stirrups spaced at 2.5 inches on center. The NM-O rebar cage prior to concrete casting is shown in Figure 2.4. The all-thread rods that are tack welded to the longitudinal rebar of the column are used to connect instrumentation.

The reinforcement for specimen LE-O, with FGSS connectors in the pier cap, is shown in Figure 2.5. The pier cap was 9-ft. long, 2-ft. deep, and 2-ft. wide. The material properties for the RC components and the repair are given in Table 2.1.

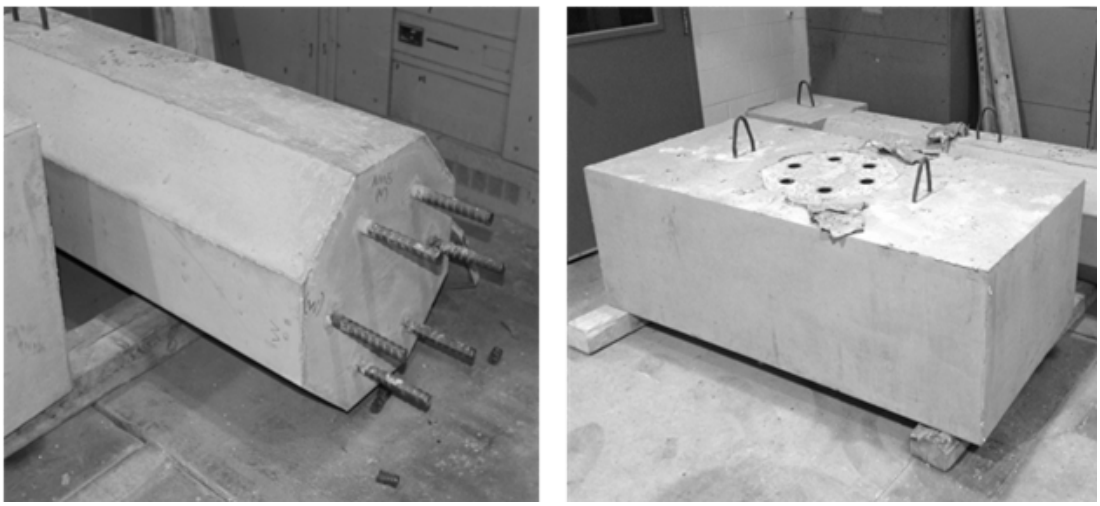

(a) (b)

Figure 2.2 Precast column-to-footing specimen NM-O prior to grouting: (a) column, (b) footing

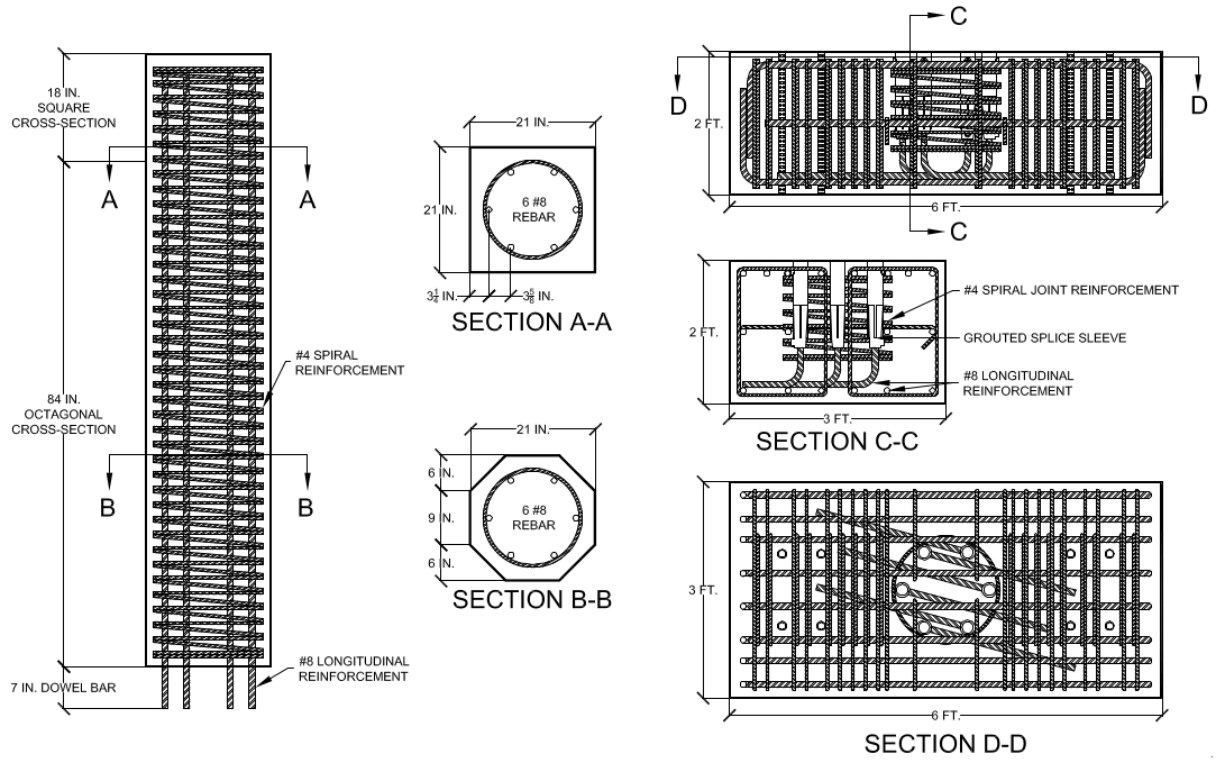

Figure 2.3 General design and detailing of joint region for specimen NM-O

(a) (b)

Figure 2.4 Rebar cages for specimen NM-O: (a) column, (b) footing

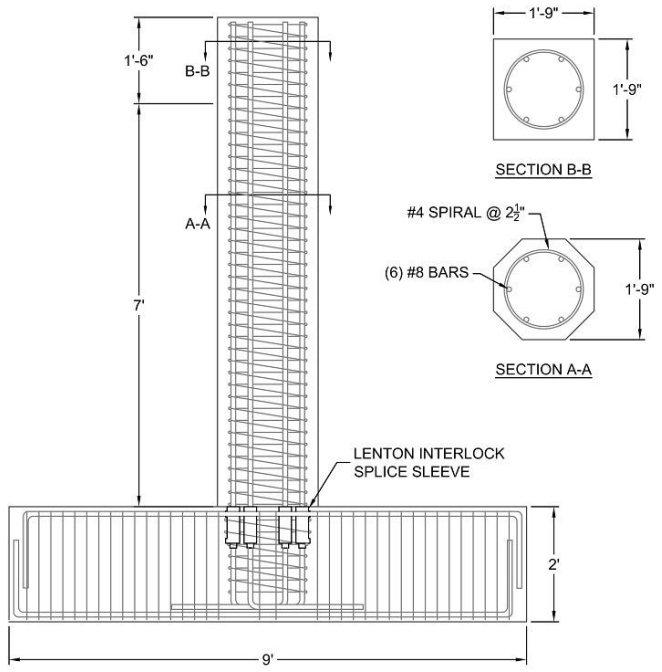

Figure 2.5 Reinforcement details for specimen LE-O

Table 2.1 As-built and repair material properties

Specimen	Bar Properties				Column Concrete Strength	Repair Concrete Strength	CFRP Jacket	
	Longitudinal (No. 8)		Headed (No. 8)					
	F_y (ksi)	F_u (ksi)	F_y (ksi)	F_u (ksi)	Test-day (ksi)	Test-day (ksi)	F_u (ksi)	E_j (ksi)
NM-O	68	93	62	86	5.5	--	--	--
NM-R	68	93	62	86	6.4	7.5	100	9000
LE-O	68	93	62	86	6.0	--	--	--
LE-R	68	93	62	86	6.1	7.0	100	9000

2.2 Test Setup

All the as-built and repaired specimens were tested in the University of Utah structures laboratory. The reactions for the test specimens were achieved by anchoring the specimens to the strong floor with 150-ksi high strength steel, 1-in. diameter threaded rods. Each end of the footing was connected with eight high-strength rods, four of which ran through PVC pipes embedded into the concrete, and four of which were outside the concrete. These rods were then tensioned prior to testing to prevent the specimens from rocking or slipping on the strong floor. The lateral load was applied to the test specimens 96 inches above the top of the footing. This point represents the theoretical inflection point of a bridge column that is subjected to double curvature. The lateral load system consisted of an actuator, a load cell, and a spherical bearing connection, as shown in Figure 2.6. The hydraulic actuator had a capacity of 120 kips and was threaded into a load cell, which in turn was attached to the specimen through a steel rod and spherical bearing.

The axial load was self-contained within the specimen, where the reactions were provided from the top of the column and the bottom of the footing, as shown in Figure 2.6. A 500-kip hydraulic actuator was used to apply the axial load, which was located on top of the column and rested on a spherical bearing plate, which allowed biaxial rotation. At the base of the footing there was a 10-in. wide by 3-in. thick plate that was pulled against the bottom of the footing by the axial load rods, which were tensioned by the actuator. The axial load rods, which connected the W-section on top of the axial actuator to the base plate, were pinned at the base plate to allow rotation of the rods while the specimen was displaced horizontally.

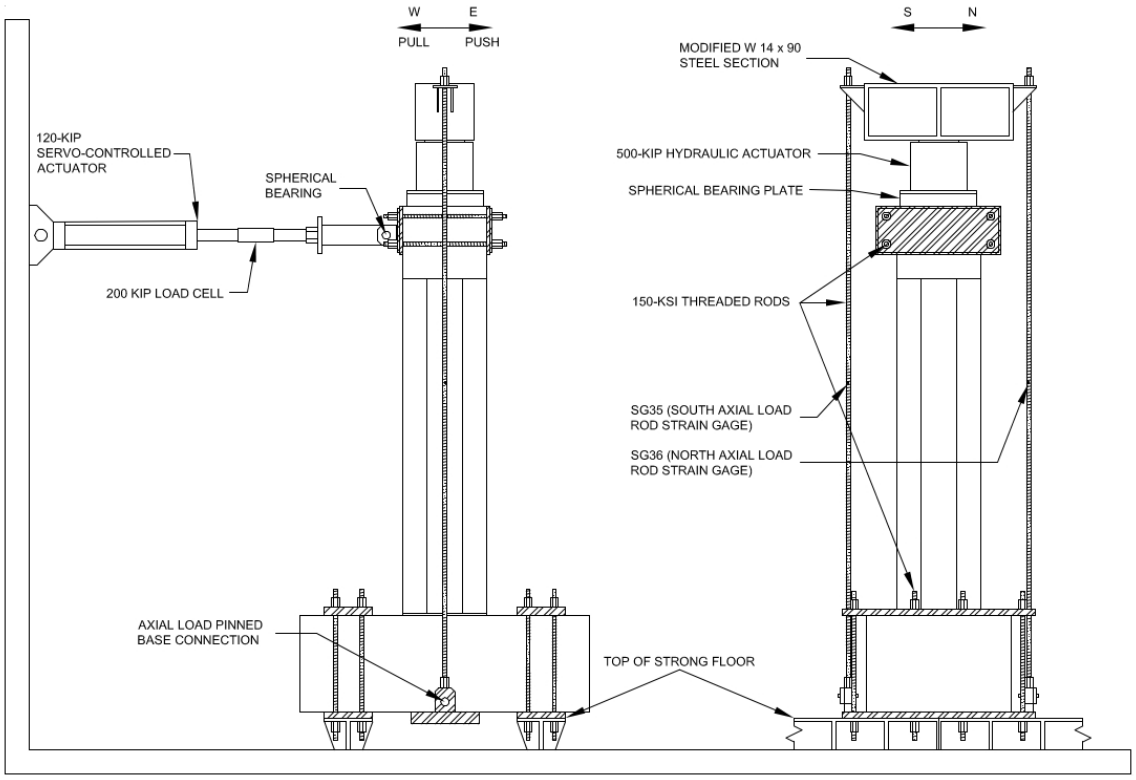

Figure 2.6 Test setup

2.3 Loading Protocol

All tests were conducted with a displacement controlled, reversed quasi-static cyclic lateral loading protocol. The applied lateral displacement history used was the same for all tests so that the hysteretic behavior could be easily compared. The applied lateral displacement history is shown in Figure 2.7. The first peak displacement used corresponds to half of the predicted yield displacement of the as-built specimens. Each subsequent peak displacement is an integer multiplier of the yield displacement. Each peak displacement was carried out for two cycles, where each cycle consisted of the peak displacement in both the positive and negative direction. This applied lateral loading protocol follows the recommendations of ACI Committee 374 [13]. The axial load applied was designed to remain constant at 6% of the axial load capacity of the column. During testing, fluctuation in the axial load as the specimen was displaced was observed. This variation in axial load was captured by strain gauges located on the axial load rods. The variation in axial load was always an increase as the specimen was displaced; from strain gage data it appears that this variation was small.

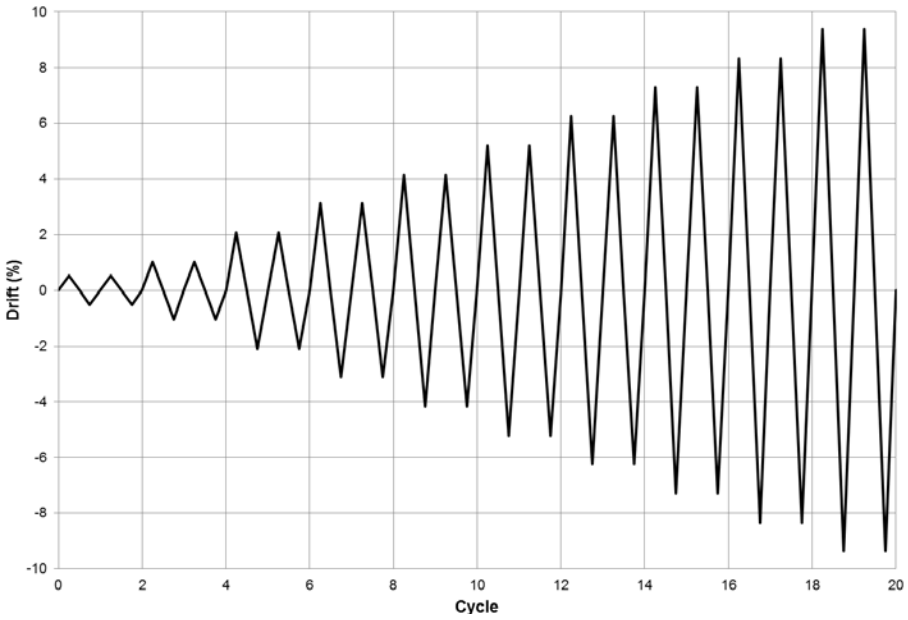

Figure 2.7 Applied lateral displacement history

3. EXPERIMENTAL RESULTS FOR AS-BUILT JOINTS

The measured response of the as-built specimens under the applied lateral displacement history is discussed in this section.

3.1 As-Built Column-to-footing Joint NM-O

Specimen NM-O was a precast concrete column-to-footing assembly that had six GGSS connectors located in the footing. The hysteretic response of this specimen is shown in Figure 3.1, and the damage condition during the final displacement step of 7 inches and after testing is shown in Figure 3.2. It can be seen from the hysteresis curves that the ultimate load achieved during the test was 38.8 kip; the ultimate drift achieved was 6.42%, and the displacement ductility was equal to 6.1. The failure mode of the specimen was crushing of the column concrete followed by longitudinal rebar facture. The east extreme longitudinal bar fractured during the first cycle of the 7-in. displacement step, approximately 3 inches above the top of the footing. The lateral load capacity in the west direction was severely diminished once the east longitudinal rebar fractured. The lateral load capacity in the west direction, after the longitudinal rebar fractured, dropped to 65% of the ultimate lateral load capacity. A plastic hinge is evident at the column-footing interface of specimen NM-O; spalling extends up the column for a distance of 8 to 12 inches on the west and east extreme column faces. Structural cracking of the column occurred at three levels located approximately 6 inches, 10 inches, and 14 inches above the footing. The maximum crack width at the 6 in., 10 in., and 14 in. levels was 0.050 inches, 0.025 inches, and 0.030 inches, respectively. Cracking extended up the column higher than 14 inches but remained hairline in width throughout testing in this region.

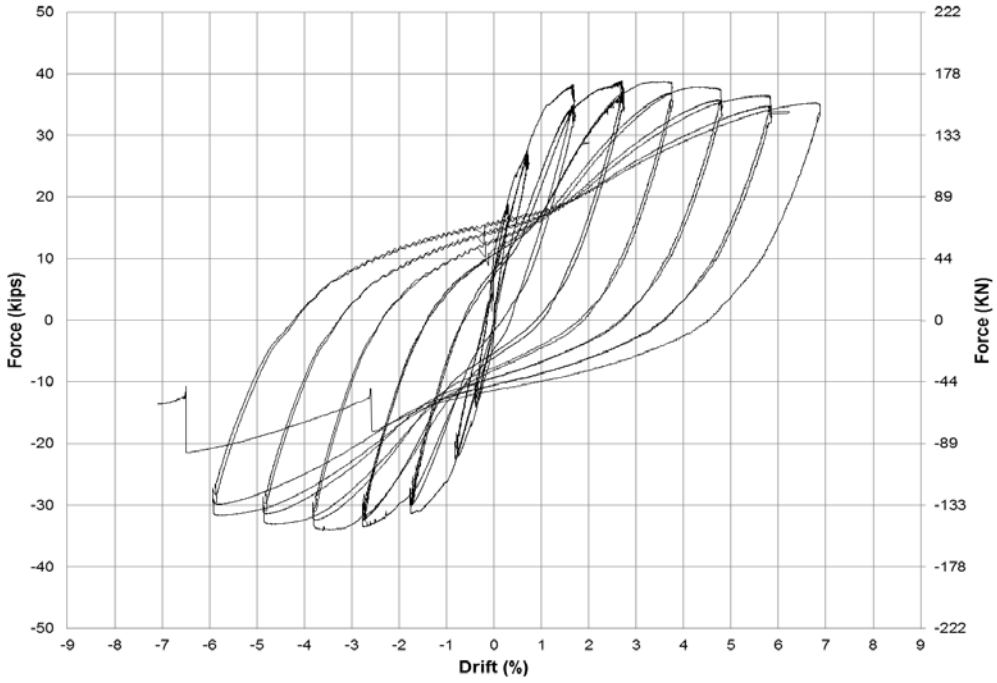

Figure 3.1 NM-O hysteresis curve

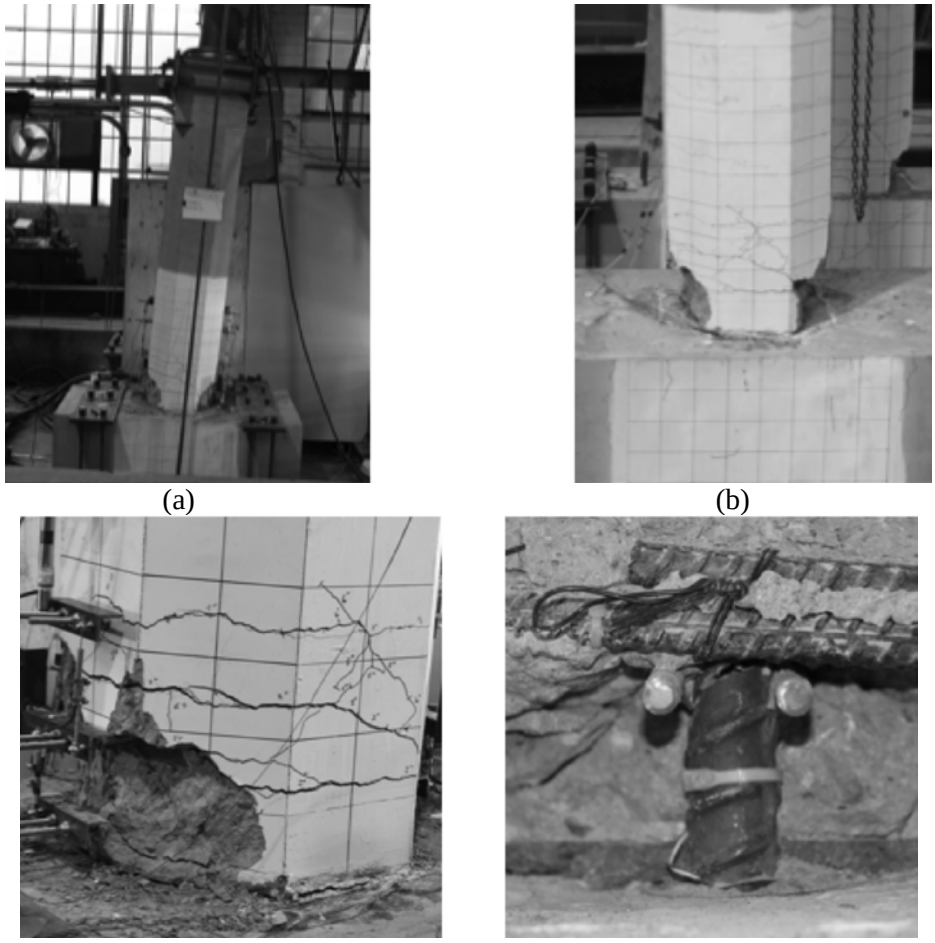

Figure 3.2 Final damage of specimen NM-O: (a) ultimate displacement of 7 inches, (b) column and footing cracking, (c) plastic hinge region, (d) fractured east longitudinal rebar

3.2 As-built Column-to-pier cap Joint LE-O

The failure mode of specimen LE-O was fracture of an extreme longitudinal bar. The extreme west longitudinal bar fractured in LE-O. Once the extreme longitudinal bar fractured, the lateral load capacity of the specimens dropped below 20% of the ultimate load capacity. From the hysteresis curves, shown in Figure 3.3, the ultimate load achieved during the test was 37.7 kip; the ultimate drift achieved was 6.50%, and the displacement ductility was equal to 5.8. A very well developed plastic hinge was formed at the column-to-pier cap interfaces where extensive spalling and cracking occurred, as shown in Figure 3.4. Major structural cracking was isolated to three distinct heights from the footing or pier cap interface, where the highest crack was located 12 inches up the column for LE-O; these crack widths ranged from 0.016 to 0.060 inches.

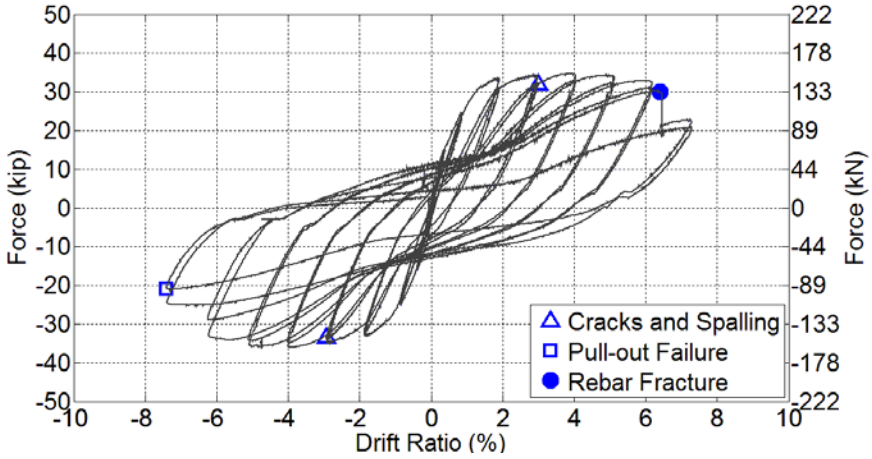

Figure3.3 Hysteresis response of specimen LE-O

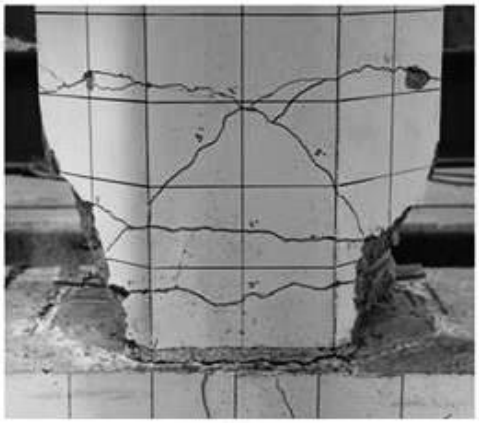

Figure 3.4 Final damage of specimen LE-O showing plastic hinge region

4. DESIGN OF THE REPAIR AND EXPERIMENTAL RESULTS

After testing as-built specimens NM-O and LE-O, a repair strategy was developed to restore the diminished load capacity of the specimens. The same repair procedure was employed on both NM-O and LE-O. Once repaired, NM-O and LE-O were renamed as repaired specimens NM-R and LE-R, respectively. Both NM-O and LE-O experienced longitudinal rebar fracture of extreme bars.

4.1 Repair Design

The objective of the repair was to re-establish the load and displacement capacity of the column-to-footing and column-to-pier cap assemblies by relocating the plastic hinge region away from the original damage location adjacent to the interface of the column with the connecting element (footing for NM-O and pier cap for LE-O). To achieve a successful repair, the original plastic hinge region must be strengthened sufficiently to withstand additional shear and moment demand that the plastic hinge relocation will produce. With reference to Figure 4.1, the bending moment that causes plastic hinge formation, M_{PH}, must be reached at the desired plastic hinge location, and a bending moment referred to as, M_{joint}, must be resisted at the column-footing (or column to pier cap) interface. M_{PH} can be determined from a sectional analysis or from test results (as in the present case).

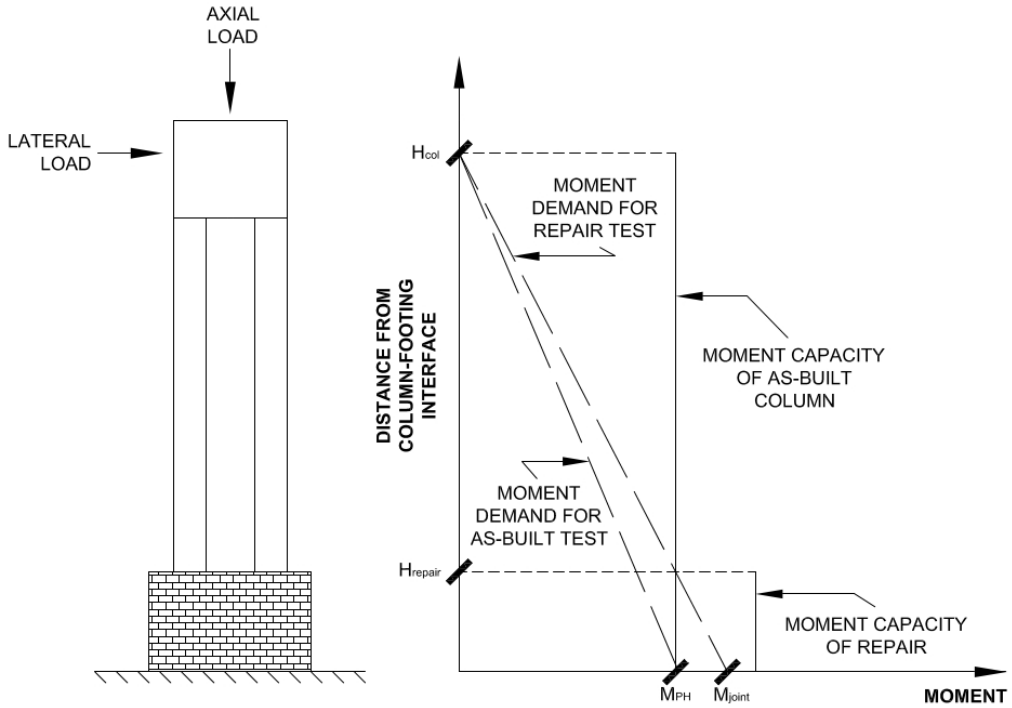

Figure 4.1 Graphical representation of design loads for simplified design procedure

M_{Joint} is proportional to the height of the repair, H_{repair}, and the height of the column from the point of inflection to the column-footing (or column-pier cap) interface, H_{col}, as shown in Eq. (4.1).

$$M_{joint} = \frac{M_{PH}}{(1 - \frac{H_{repair}}{H_{col}})} \quad (4.1)$$

Using the minimum possible repair height is advantageous for limiting the moment demand at the column-footing (or column-pier cap) interface and for decreasing the rotational demand on the column for a given displacement. The height of the repair must be long enough to relocate the new plastic hinge to a minimally damaged (or undamaged) cross-section.

From the bending moment M_{joint}, the shear that must be resisted in order to achieve plastic hinge relocation, V_{PHR}, can be found from Eq. (4.2):

$$V_{PHR} = \frac{M_{joint}}{H_{col}} \tag{4.2}$$

Similar to moment demand, the shear demand is directly related to the height of the repair. This relationship can be obtained by substituting Eq. (4.2) into Eq. (4.1) as:

$$V_{PHR} = \frac{M_{PH}}{H_{col} - H_{repair}} \tag{4.3}$$

From both Eqs. (4.1) and (4.3) it can be seen that the repair height, H_{repair}, should be kept to a minimum to reduce the moment demand on the repair and the shear demand on the column. The shear capacity of the repaired cross-section will be much higher than the shear capacity of the as-built section. Since the shear demand is constant along the height of the column, it is likely that the shear capacity will be controlled by the as-built section above the repair. The shear capacity of the as-built section must be greater than V_{PHR}.

The height of the repair was designed to cover the plastic hinge length of the as-built specimen and to cover all of the structural cracking, larger than 0.01 in., while remaining as short as possible. This led to a nominal repair height of 18 inches. The 18-in. nominal repair height, ranged from 19 to 20 inches when the construction process was completed. This increase in height was due to the 0.5-in. gap that was intentionally left between the CFRP wrap and footing (or pier cap). This gap is provided to decrease the risk of the wrap bearing on the footing (or pier cap) concrete. Once the height of the repair is determined, the load associated with plastic hinge relocation, in terms of shear and moment, is established. The shear strength of the as-built column section must be checked against V_{PHR}. Since the repair is developed for specimens with fractured or highly damaged longitudinal rebar, the tension transfer between column and footing (or column and pier cap) must be re-established through the repaired cross-section.

To achieve these design criteria, a repair was developed, for both specimens NM-O and LE-O, which increased the original plastic hinge region from a 21-in. octagonal cross-section to a reinforced 30-in. diameter circular cross-section. Additional reinforcement was provided in the form of headed steel rebar. The headed steel bars were designed to increase the flexural strength of the repair and re-establish the tension transfer between the column and footing (or pier cap). Additional shear reinforcement was provided in the form of a unidirectional CFRP wrap. The CFRP wrap was designed to provide shear strength and confinement to the repaired cross-section. The confinement provided by the CFRP wrap increases the capacity of the repaired region by increasing the compressive strength and strain capacity of the concrete within the repair.

The repair details for specimen NM-O are shown in Figure 4.2; the details for specimen LE-O were identical. There are three components for the repair that must be designed: headed rebar, CFRP wrap, and non-shrink concrete. As usual with design, the different repair components rely upon one another, making the design process iterative. The headed steel bars are designed to increase the moment capacity of the repaired cross-section to a value larger than M_{joint}. The contribution of the as-built longitudinal rebar can be conservatively ignored when determining the repaired cross-section moment capacity. This

assumption should be made when longitudinal bars have fractured or buckled in the as-built column prior to repair. The moment capacity provided by the headed rebar is controlled by the area of steel that is provided and the moment arm of the steel. Placement of the headed rebar fixes the moment arm of each rebar and should be determined from several design criteria. First, a minimum clear spacing between the as-built column and the center of the headed rebar should be maintained to allow space for drilling into the footing; in the present case this was 2 inches. Space should also be provided between the headed rebar and the CFRP wrap to allow proper bonding of the CFRP composite to the concrete and development of the headed rebar. The smallest diameter possible for the CFRP wrap should be selected to facilitate an economical design and to minimize interference with surrounding objects when the repair is installed in the field. From these design criteria, the placement of the headed rebar and the diameter of the CFRP jacket can be designed iteratively. In practice, the headed rebar should be distributed around the repair evenly since the direction of lateral load from a future earthquake is not known.

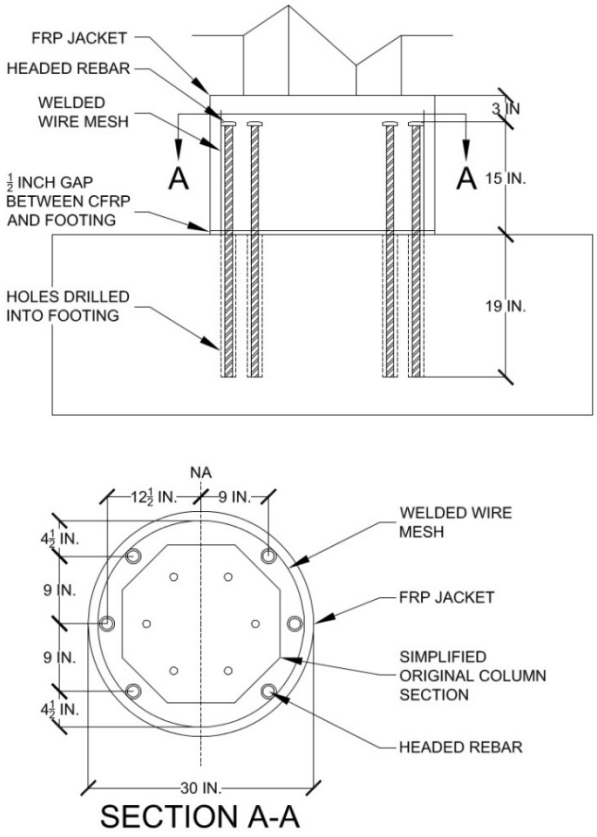

Figure 4.2 Repair design details for specimen NM-O

With an estimate of the number of headed bars and placement, the minimum amount of the headed bar area can be determined from Eq. (4.4) as:

$$M_n = A_s * f_y * \left(d - \frac{A_s * f_y}{1.70 * f'_c * b_w} \right) > M_{joint} \qquad (4.4)$$

where M_n is the nominal flexural capacity of the repaired section, neglecting compression steel, and assuming zero axial load. Neglecting the axial load contribution for the flexural strength capacity of the repaired cross-section is conservative. A_s is equal to the cross-sectional area of the headed rebar in tension, f_y is the nominal yield strength of the headed rebar, d is the distance from the centroid of the

headed rebar to the neutral axis, f_c' is the nominal compressive strength of the repair concrete, and b_w is the effective width of the repair. An appropriate margin of safety should be maintained between the flexural capacity of the section and the demand. These design equations lead to six No.8 Grade 60 headed bars placed, as shown in Figure 4.2, with three headed bars on each side of the repaired section.

The length of epoxy anchorage into the footing and amount of embedment into the repair concrete must also be designed to provide proper development length. Since the repair procedure is for bridge columns that are exposed to corrosive environments, a clear cover of 3 inches was provided between the top of the headed bars and the top of the repair concrete [14]. This cover requirement left a development length of 15 inches for the headed rebar in the repair concrete. The required development length is determined from Eq. (4.5) as:

$$l_{dt} = \left(\frac{0.016 * \psi_e * f_y}{\sqrt{f_c'}}\right) * d_b > 8 * d_b \text{or } 6 \text{ in.} \tag{4.5}$$

where l_{dt} is the required development length for the headed rebar, ψ_e is equal to 1.0 for non-epoxy coated rebar, and d_b is the diameter of the headed rebar. For the No. 8 rebar specified and a conservative f_c' of 4000 psi, the required development length is 12.0 inches, which is less than the 15 inches provided. Therefore, the design is adequate. Similar to the development length of the headed rebar in the repaired concrete section, the headed rebar must develop in the epoxy anchorage within the footing (or pier cap). The required development length for the epoxy anchorage, l_d, is determined from Eq. (4.6):

$$l_d = \frac{A_b * f_y}{d_b * \pi * \tau} \tag{4.6}$$

where A_b is the cross-sectional area of one headed bar and τ is equal to the specified bond strength of the epoxy used. The epoxy used for the repair was Hilti HIT-RE 500-SD epoxy, which has a bond strength of 1400 psi [15]. Using No. 8 headed rebar, the required development length is 12.2 inches, which is less than the 19 inches provided; therefore, the design is sufficient.

The repair concrete that was used to fill the void between the damaged column and CFRP wrap for specimens NM-R, and LE-R was designed as non-shrink concrete. The mix design is shown in Table 4.1. The amount of expansion is controlled by the ratio of Komponent cement to Portland Concrete Cement (PCC). Komponent is intended to produce non-shrink concrete when proportioned at 15% of the cementitious materials.

Table 4.1 Repair concrete mix design for NM-R and LE-R

Cementitious materials			Water		Aggregates (lb/yd @ SSD)		Additives (oz/yd)	
Komponent (lb/yd)	PCC (lb/yd)	Percent Komponent (%)	Cold water (lb/yd)	Water to cement ratio (%)	Point 3/4 in.	Point sand	Daravair (air entrainer)	Glenium 30-30 (super plastisizer)
92	599	13	280	41	1600	1060	6.5	49

The purpose of the CFRP jacket is to provide confinement and shear strength to the original plastic hinge region. Proper confinement increases both the strain capacity of the confined concrete and its compressive strength. Research has shown that a minimum jacket thickness and associated confinement are required to prevent strain softening of CFRP confined concrete [16]. Therefore, a jacket thickness was provided to ensure strain hardening of the concrete within the jacket. The jacket was also designed to withstand all of the shear demand, V_{PH}, over the length of the repair. Although the as-built column has

sufficient shear capacity to resist V_{PH}, the original plastic hinge region needs shear strengthening due to concrete crushing and the spiral yielding during the initial test of the as-built specimens.

From previous research [16], the CFRP jacket thickness, $t_{j,sh}$, required to ensure strain hardening behavior of the confined concrete and provide proper confinement is determined by Eq. (4.7):

$$t_{j,sh} = \left(\frac{f_{co}}{E_f}\right) * \left(\frac{H_c * \lambda_{SH}}{4 * C_{sh}}\right) \tag{4.7}$$

where f_{co} is the unconfined concrete compressive strength; E_f is the CFRP modulus of elasticity; H_c is the diameter of the CFRP jacket; λ_{SH} is a factor accounting for the aspect ratio of the CFRP section and is equal to 12 for circular cross-sections; and C_{sh} is the jacket confinement ratio coefficient, which is equal to 1.0 for circular cross-sections. The CFRP jacket thickness required for shear strengthening of circular column sections in plastic hinge regions, $t_{j,v}$, was determined from Eq. (4.8) as [4]:

$$t_{j,v} = \frac{\frac{V_{PH}}{\Phi_v} - (V_c + V_s + V_p)}{\frac{\pi}{2} * 0.004 * E_f * H_c} \tag{4.8}$$

where V_{PH} is the column shear demand; Φ_v is the shear capacity reduction factor, which was taken as 0.85; and $V_{c,}$, V_s, and V_p are the shear capacity contribution of the concrete, shear reinforcement, and axial load, respectively. Due to the damage state of the original plastic hinge region, $V_{c,}$ V_s, and V_p can all conservatively be taken as zero.

The total jacket thickness needed for the repair, $t_{j,total}$, is obtained by using Eq. (4.9):

$$t_{j,total} = \left(t_{j,sh} + t_{j,v} + t_{j,shell}\right) \tag{4.9}$$

where $t_{j,shell}$ is an additional term for the CFRP shell required as formwork for the repair concrete. For specimens NM-R and LE-R a total of four CFRP layers were provided: two layers were provided to prevent strain softening and provide confinement, one layer was provided for shear strength, and one layer was provided as a shell for the repair concrete. The shell layer was used as a construction aid to maintain the circular cross-sectional shape. Each CFRP layer has a nominal thickness of 0.04 inches. The material properties for the RC components and the repair were provided in **Table 2-1**.

4.2 Repair Procedure

The first step in the repair was creating the CFRP wrap from unidirectional SikaWrap Hex 103C fibers oriented in the hoop direction and Sikadur Hex 300 Epoxy. The impregnation process was done by hand using a paint roller and abrasive metal roller. Once saturated, the excess resin was scraped off the CFRP composite using a rubber tool. To create a stay-in-place formwork for the repair concrete, a single layer of 18-in. wide CFRP composite was wrapped and cured around a 30-in. diameter circular sonotube. After curing, the CFRP shell was cut into two half cylinders to simulate the way this procedure would be executed in the field.

Once the shell was placed around the column, it was spliced with two 12-in. long pieces of CFRP composite for the height of the repaired column. The 12-in. splice length was determined to provide proper development of the fibers on either side of the splice. Three additional 100-in. long CFRP layers were wrapped around the shell. This length was used to provide an overlap of 6 inches for each layer. The sonotube was left inside the CFRP shell to provide rigidity while the additional layers of CFRP composite were applied; it was removed once all layers had cured. **Figure 4-3** shows the steps involved in preparing the CFRP shell.

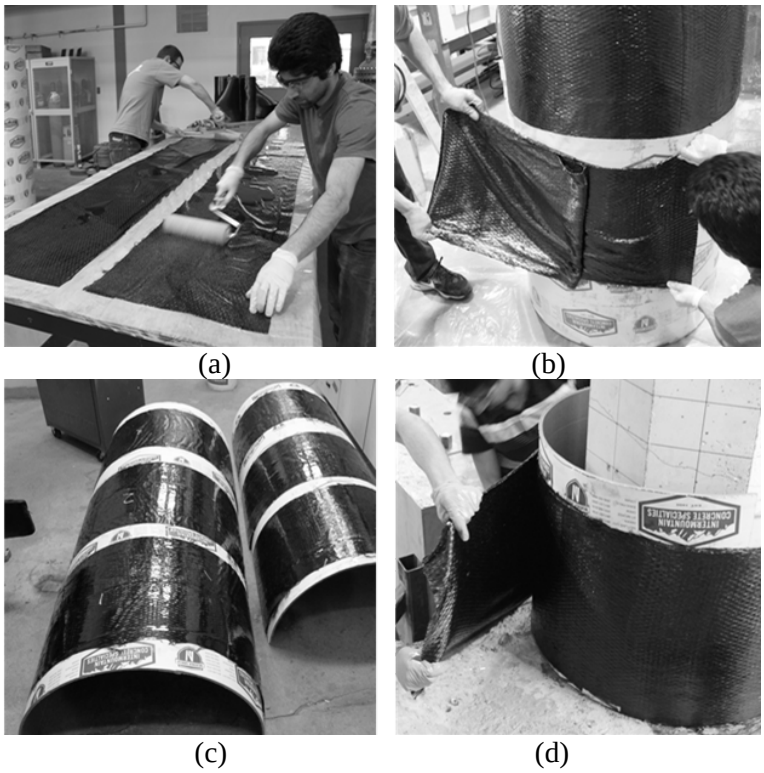

Figure 4.3 CFRP composite preparation: (a) saturation, (b) making shells, (c) split prefabricated shells, (d) wet layup

While the CFRP shells were curing, the holes for the post-installed headed bars were core-drilled into the footing. The hole diameter was 1.25 inches, which provided a radial clearance of 0.125 inches between the headed rebar and the hole. Hilti HIT-RE 500-SD epoxy was injected into the hole using a Hilti dispenser to avoid the formation of air voids. Figure 4.4 shows the steps involved in preparing the headed rebar. Once the CFRP shell and epoxy for the headed rebar had fully cured, non-shrink concrete was added to the space between the column and CFRP shell. The concrete was vibrated to minimize the amount of air voids left within the repair concrete. A 0.5-in. gap between the CFRP shell and the footing was maintained. The repair concrete was cured for at least 28 days before testing.

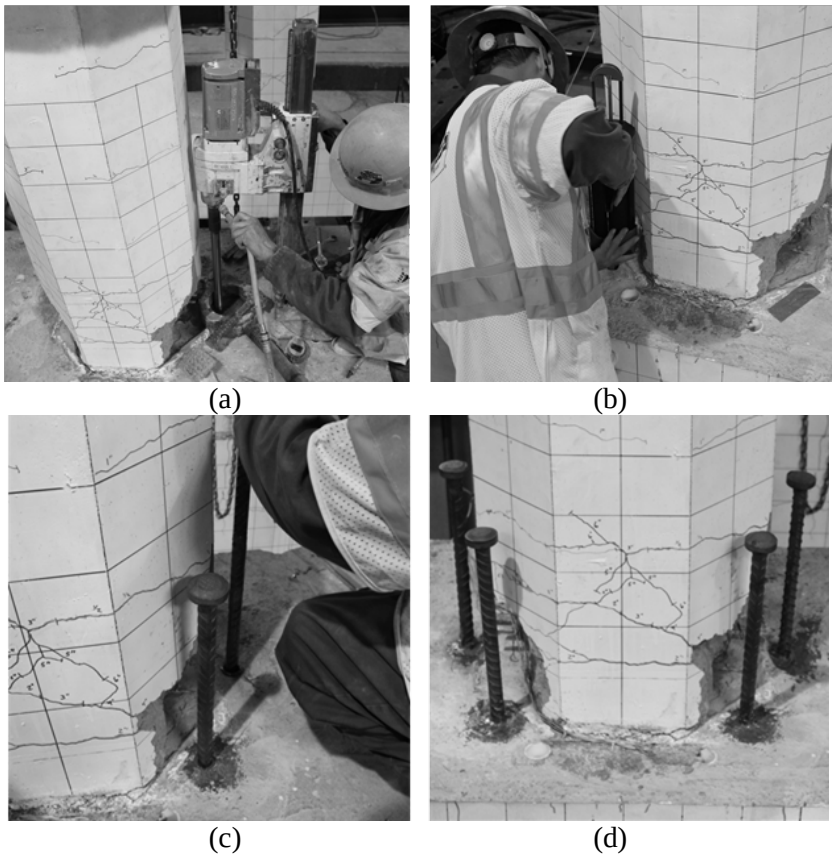

Figure 4.4 Headed rebar installation: (a) core drilling, (b) epoxy injection, (c) inserting rebar, (d) after installation

Figure 4.5 shows the steps involved in casting the concrete for the repair process. For specimen LE-O, there was wood formwork on the edge of the pier cap, as shown in Figure 4.6. This wood formwork was put in place to extend the width of the pier cap since the diameter of the repair (30 inches) was larger than the width of the pier cap (24 inches).

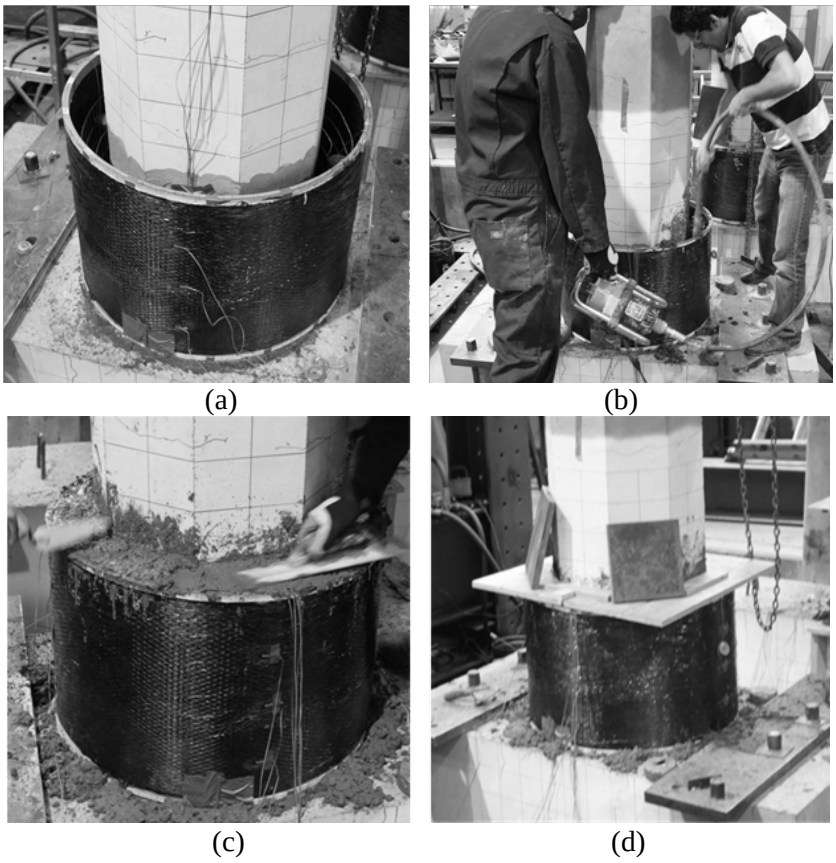

(a) (b)

(c) (d)

Figure 4.5 Repair concrete: (a) before casting, (b) vibrating, (c) finishing concrete after casting, (d) wooden formwork and weights

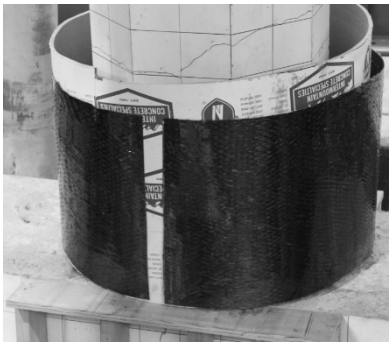

Figure 4.6 Split CFRP shell for specimen LE-R

4.3 Experimental Result of Repaired Joints

The measured response of the repaired specimens under the applied lateral displacement history is discussed in this chapter. The test assembly and loading protocol used to test the as-built specimens NM-O and LE-O were also used to test the repaired specimens NM-R and LE-R.

4.3.1 Repaired Column-to-footing Joint NM-R

The objective of repairing specimen NM-O was to restore the diminished load and displacement capacity through plastic hinge relocation. Plastic hinge relocation was achieved after the repair and is shown in Figure 4.7. The hysteretic response and force-displacement envelope of NM-R is shown in Figure 4.8 and Figure 4.9, respectively. From these figures it is seen that both the load and displacement capacity of NM-R were restored. The ultimate drift achieved was 6.96%, and the ultimate load was approximately 45.56 kips. The displacement ductility that NM-R achieved was 7.52 when displaced to the east and 4.15 when displaced to the west.

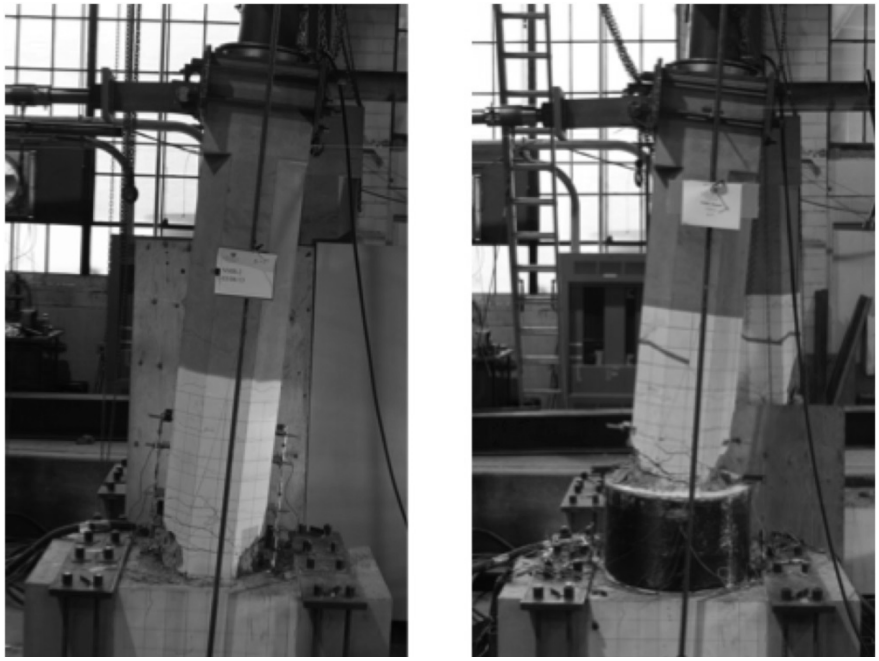

(a) (b)

Figure 4.7 Specimens displaced to the east at the maximum displacement: (a) NM-O, (b) NM-R

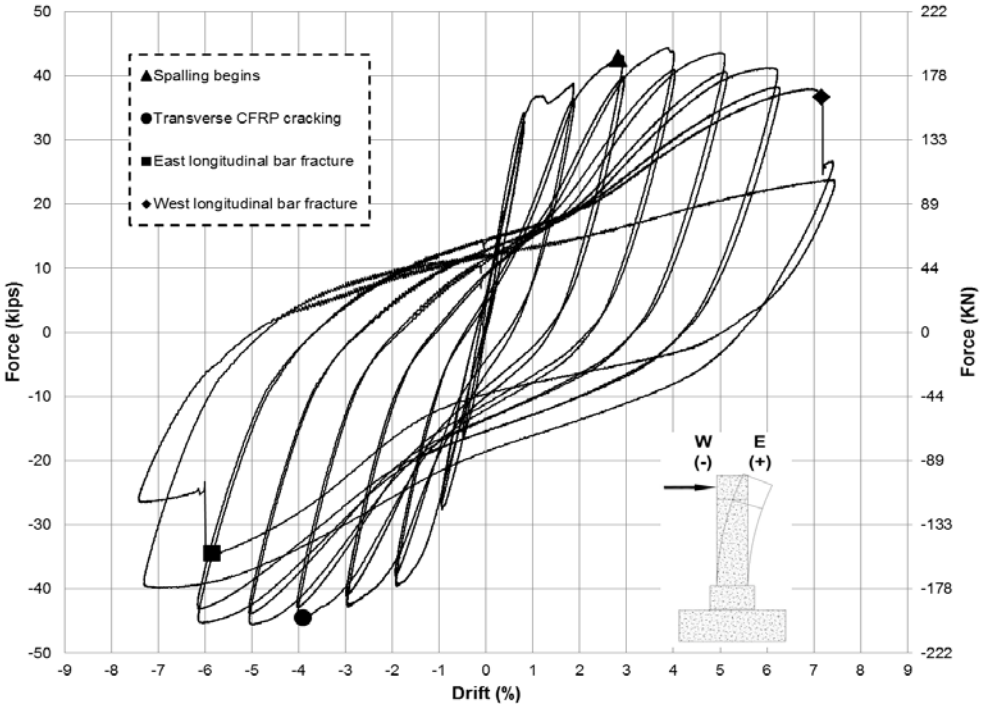

Figure 4.8 NM-R repaired specimen hysteresis curve

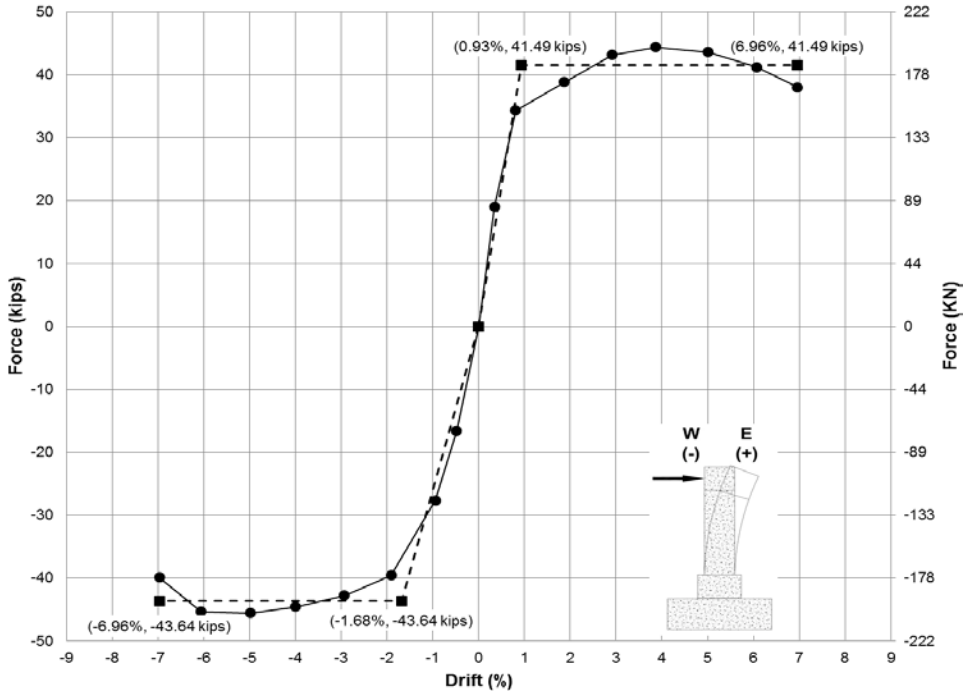

Figure 4.9 NM-R repaired specimen backbone curve

The displacement ductility when displaced to the west is approximately 55% of the displacement ductility when displaced to the east. The loading protocol displaces the specimen to the east before the west for each cycle, degrading the stiffness of the specimen, which causes this difference in displacement ductility. The average ductility, calculated from an averaged envelope curve of repaired specimen NM-R, is 5.95.

Repaired specimen NM-R reached an ultimate lateral load during the 4-in. to 5-in. displacement step, and experienced longitudinal rebar fracture of both the west and east extreme bars during the 7-in. displacement step. The fracture locations for the west and east longitudinal bars were 3 inches and 4.5 inches, respectively, above the top of the repair. Both bars fractured during the 7-in. displacement step. The west rebar fractured in tension during the first cycle, and the east rebar fractured in tension during the second cycle. The east longitudinal rebar fractured in both the NM-O test and the NM-R test. The fracture location of the east longitudinal rebar during the NM-R repaired joint was 21.5 inches above the fracture location during the NM-O as-built joint. The distance between the two fracture locations corresponds to 51% of the design development length for a No. 8 bar [14]. This short development length shows that the CFRP jacket was able to exert significant confining forces on the longitudinal steel reinforcement.

Transverse cracking of the CFRP shell was observed during the test of specimen NM-R, as shown in Figure 4.10. The crack began during the 4-in. displacement step and grew during each subsequent displacement step. At completion of the test, the crack extended halfway around the circumference of the CFRP jacket. The hysteretic response of the specimen was unaffected by the transverse CFRP crack, which was located 3 to 4 inches below the top of the repair, corresponding to the top of the internal headed rebar. The onset of transverse CFRP cracking can be seen from the curvature profile obtained from the experiments in Figure 4.11, which shows the maximum and minimum curvatures during the 0.5-in. to 4-in. displacement steps. There are two curvature values plotted for each displacement step in the east and west directions. The first value is an average curvature value from the top of the footing to the top of the repair. The second value is an average curvature value from the top of the repair to 9.56 inches up the column. From this plot, it can be seen that the curvature of the wrapped section is very small when compared with the column, indicating plastic hinge formation in the column. Also, the onset of the CFRP crack can be seen by the increase in curvature of the repaired specimen when it was displaced to the west during the 4-in. displacement step.

Figure 4.10 Transverse CFRP crack at white line 3 inches below top of CFR shell

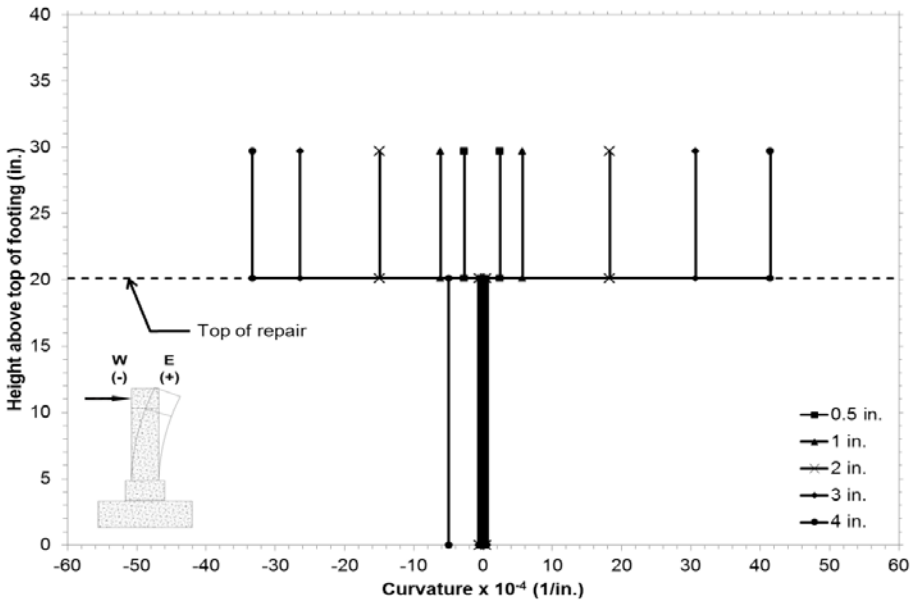

Figure 4.11 NM-R repaired specimen curvature profile up to 4-in. displacement step

Other notable events pertaining to the damage state of specimen NM-R were as follows. During the 0.5-in. displacement step, the damage observed was the opening of a crack obtained during the NM-O joint test. The crack only opened at the extreme displacement and was located 1 inch above the top of the repair. Once the specimen was at rest, the crack was measured to be hairline.

The 1-in. displacement step marked the onset of radial cracking in the repair concrete. The radial cracks originated from six of the eight column corners and were measured to be a maximum of 0.005 inches, as shown in Figure 4.12(a).

The 2-in. displacement step started with an audible event occurring during the first displacement to the east. The event can be seen in the hysteresis in Figure 4.8 as a plateau beginning at approximately 1% drift and continuing through completion of the cycle. The noise that was heard was due to relaxation of the tie-down rods that anchor the specimen to the strong floor. The unbalanced tension in the rods due to residual displacements from the original test was relieved as one of the rods shifted. This event resulted in the tie-down rods balancing the reaction forces on both sides of the specimen, subsequently making the hysteretic behavior of the test symmetrical from that point forth. New cracking occurred during this round with a 0.06-in. crack opening up 2 inches above the top of the repair on the east column face, as shown in Figure 4.12(b). A 0.025-in. crack originating 3 inches above the repair on the west face was created during the 2-in. displacement step. These cracks continued to grow throughout the test and are the beginning of the plastic hinge formation.

Spalling began during the 3-in. displacement step at the east and west corners of the column. Gapping was observed between the column and the repaired concrete section and continued to grow throughout the test sequence, as shown in Figure 4.12(c).

During the first cycle of the 4-in. displacement step, the transverse CFRP crack discussed previously originated on the east side of the repair when the column was displaced to the west. During this displacement step, shear x-cracking began on both the north and south faces, as shown in Figure 4.12(d). The x-cracks had a maximum width of 0.013 inches. Spalling of the cover concrete above the repair continued during this displacement step.

During the 5-in. displacement step, a new flexural crack was observed 10 inches above the top of the repair. When the crack was measured at rest it was hairline. The radial cracks grew considerably during this displacement step from 0.005 in. to 0.025 in. The largest radial cracks were located on the west side of the repaired section. Spalling continued during this displacement step and the shear x-cracks grew in length, as shown in Figure 4.13(a).

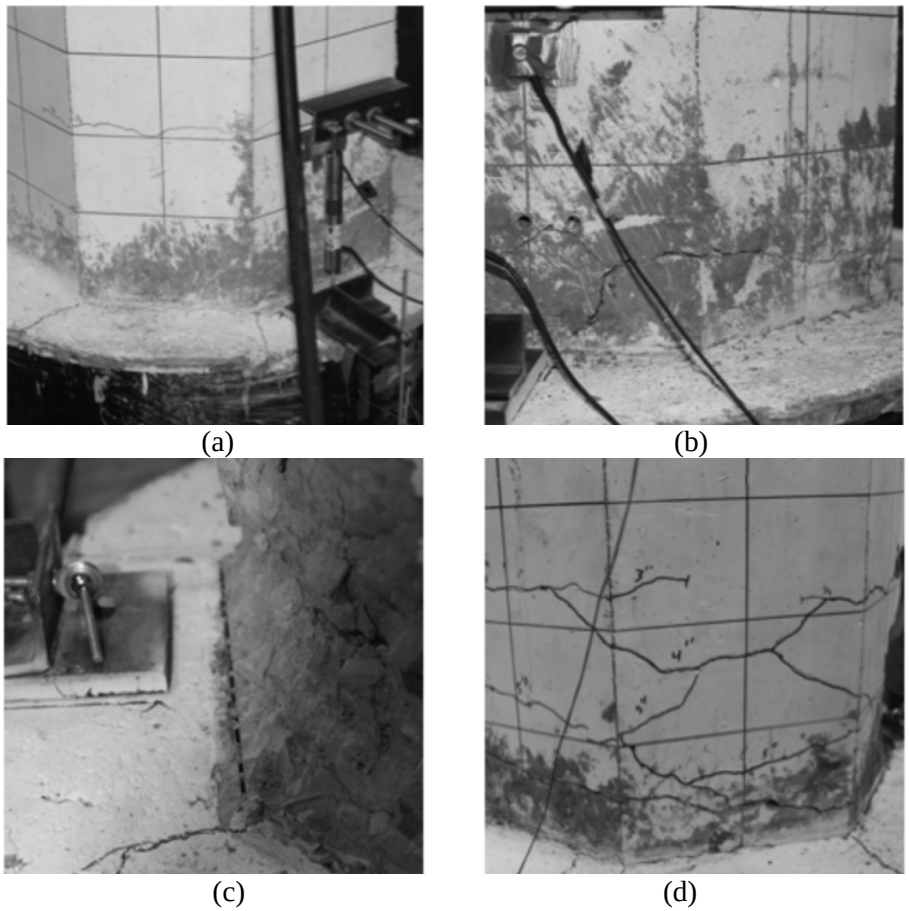

Figure 4.12 NM-R test through the 6-in. displacement step: (a) radial cracks after 1-in. displacement step, (b) first crack during 2-in. displacement step, (c) gapping at repair-column interface during the 6-in. displacement step, (d) shear x-crack after the 4-in. displacement step

No new cracks were observed during the 6-in. displacement step. The cracks located approximately 10 inches above the top of the repair increased in width from hairline to 0.1 inches and 0.025 inches on the east and west column faces, respectively. The damage state at the end of the 6-in. displacement step is shown in Figure 4.13(b).

During the 7-in. displacement step, both the west and east extreme longitudinal bars fractured. The west longitudinal bar fractured during the first cycle, and the east longitudinal bar fractured during the second cycle. In addition to bar fracture, the shear x-cracking grew on the north and south faces, measuring 0.06 inches at pause. NM-R at maximum displacement is shown in Figure 4.13(c). The final damage state of NM-R is shown in Figure 4.13(d).

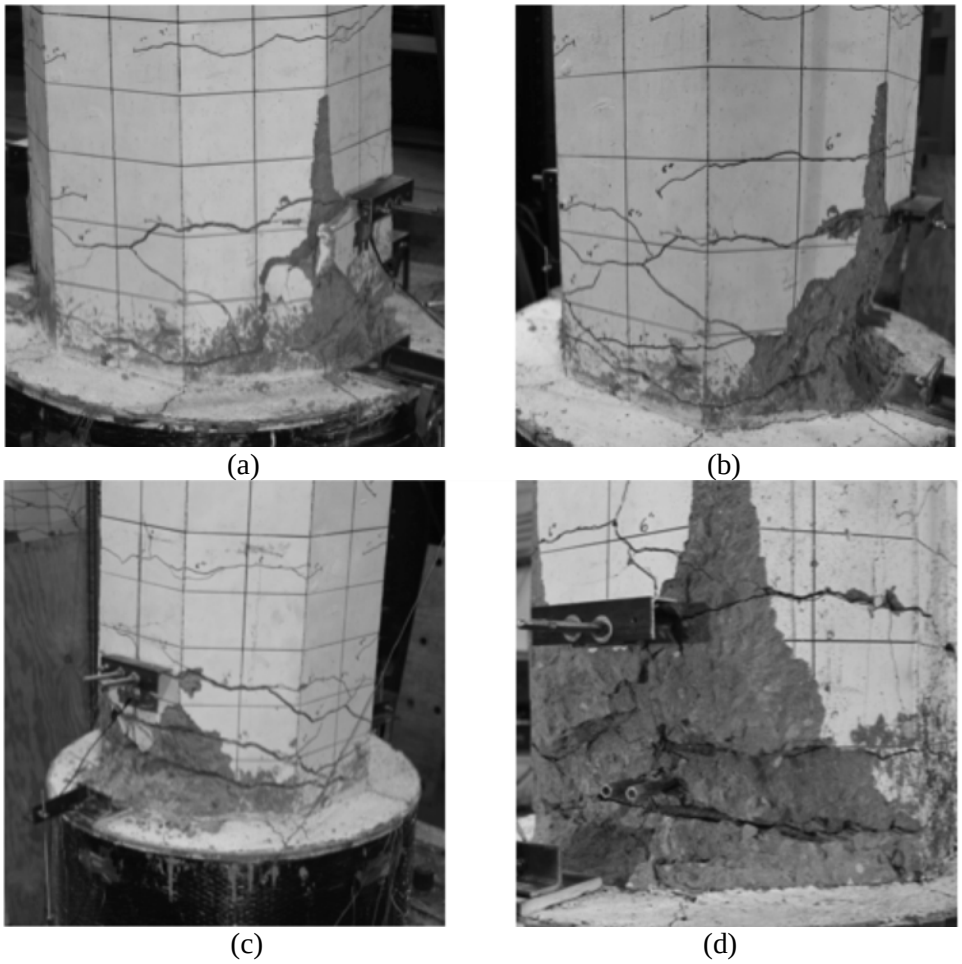

Figure 4.13 NM-R test through final damage state: (a) major spalling during 5-in. displacement step, (b) damage level after 6-in. displacement step, (c) damage state during 7-in. displacement step, (d) final damage state

The performance of the CFRP jacket during the NM-R test is studied in this section. The four layers of unidirectional CFRP composite provided sufficient shear strength and confinement to the repaired cross-section, facilitating relocation of the plastic hinge region to the top of the repair. The CFRP jacket results are highly affected by the repair concrete properties. The specimen had non-shrink concrete, which caused pre-tensioning of the CFRP jacket to a strain of 0.01% prior to testing. The strain result from testing will be compared to the effective strain capacity of the CFRP jacket. The effective strain capacity for the repair was taken as 57% of the ultimate strain capacity recorded from tensile coupon tests [17]. The CFRP strain efficiency factor accounts for strain concentrations, and the multiaxial state of stress acting on the jacket when the CFRP wrapped member is subjected to compression and bending. The concrete that filled the NM-R specimen's CFRP jacket was non-shrink concrete that pre-tensioned the jacket to 105 microstrain. This is a very small amount of pre-tensioning, accounting for less than 2% of the jacket's effective strain capacity. Transverse CFRP cracking started during the test at the 4-in. displacement step and grew throughout the subsequent displacement steps, as illustrated in Figure 4.10. Although this characteristic is of concern, the transverse cracking did not adversely affect the results of the repair.

Figure 4.14 shows the uneven vertical distribution of strain throughout the CFRP jacket during the NM-R joint test. Four different levels of strain gauges, placed at different heights above the top of the footing, are averaged together on all four sides of the CFRP jacket, giving an average top band, top, middle, and bottom strain value. The top band, top, middle, and bottom levels of strain gauges are located 16.5 inches, 14.5 inches, 9.5 inches, and 4.5 inches above the top of the footing, respectively. The maximum strain reached in the bottom, middle, and top levels is 15%, 38%, and 78% of the maximum strain reached in the top band level. Figure 4.14 shows a plateau in the strain that the wrap develops, which begins with the 4-in. lateral displacement step. The maximum lateral load was reached during the 4-in. displacement step. The peak strains for each displacement step follow the shape of the response envelope from the test, implying that the jacket strain level is controlled by load rather than displacement. The maximum strain recorded in the jacket was on the east side of the wrap at the level of the top band as 3200 microstrain, or a maximum of 50% of its effective strain capacity.

Uneven straining of the jacket, when displaced east and west, is shown in Figure 4.14. The second displacement in each cycle, corresponding to a displacement in the east direction, experiences more strain than in the first displacement. This uneven directional straining is present up to the first cycle of the 4-in. displacement step, up to an elapsed time of 4000 s, when the jacket developed the transverse crack. The cracking relieved the uneven distribution of directional strain. The onset of transverse cracking can be seen from individual strain gauge data from the top band, shown in Figure 4.15. The top band east strain gauge is engaged in both displacement directions through the first cycle of the 4-in. displacement step, at the 4% drift ratio, when transverse cracking began. Onset of the crack relieved the strain in both directions, and the CFRP wrap began to act similarly to the top band west strain gauge, as shown in Figure 4.15(a). Between displacement steps, the wrap is experiencing residual strain from dilation of the repaired concrete. Figure 4.14 and Figure 4.15 show an increase in residual strain after each displacement step. The largest increase in residual jacket strain is between the 1-in. and 2-in. displacement steps due to radial cracks, as shown in Figure 4.12(a), which caused the concrete inside the repaired section to dilate, increase the pressure on the CFRP wrap, and thereby increasing the wrap strain.

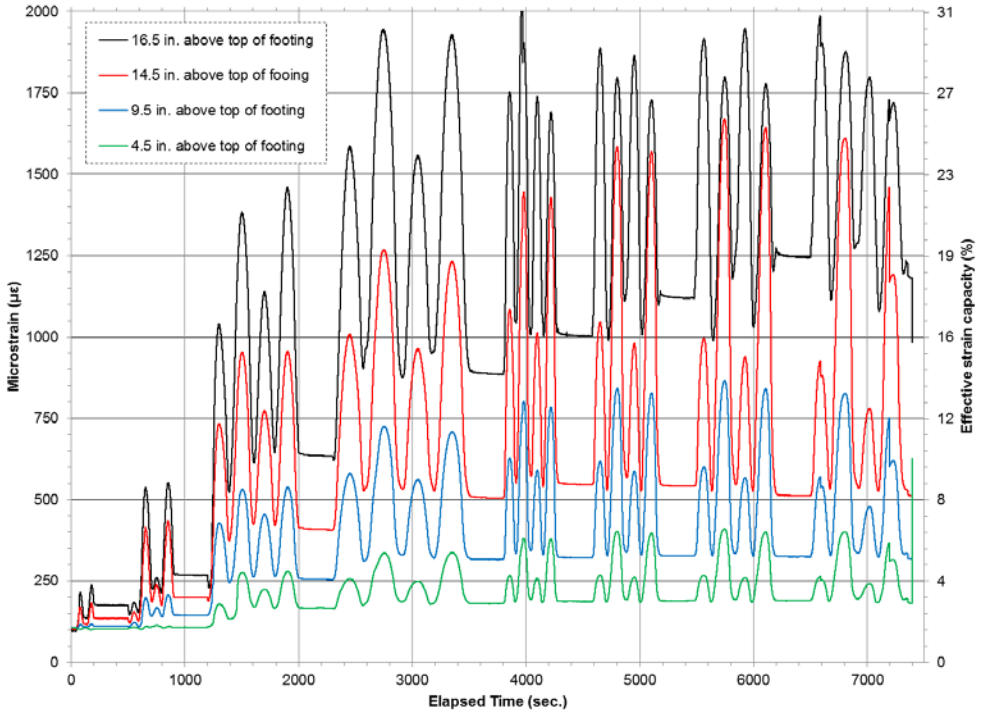

Figure 4.14 NM-R CFRP wrap strain gauge data averaged by height

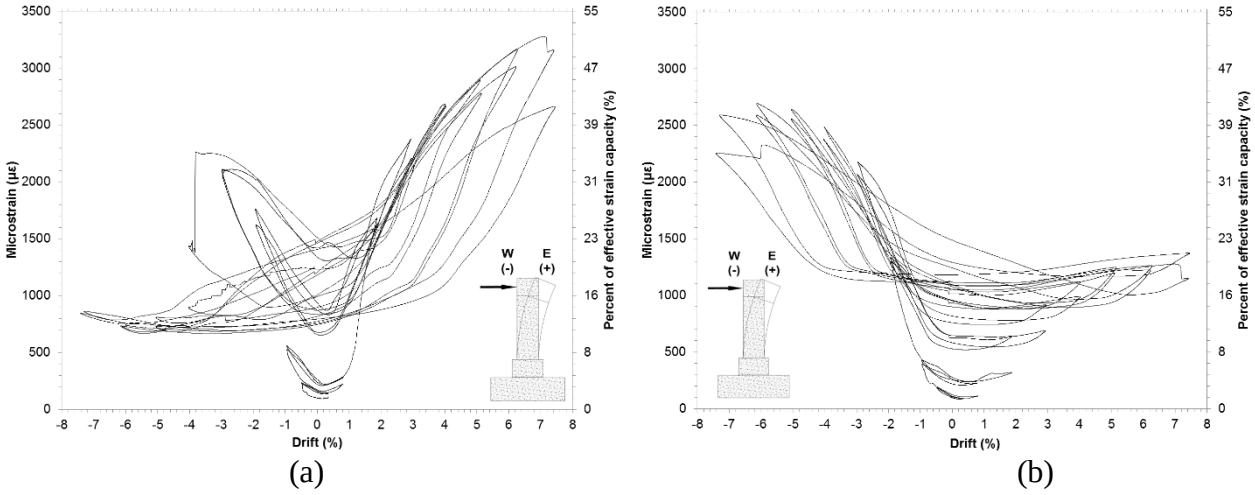

Figure 4.15 NM-R CFRP wrap strain gauge data from top 3-in. band: (a) East, (b) West

Figure 4.16 shows the uneven distribution of strain vertically throughout the jacket; the strain profile is a plot of the strain gauge height above the footing versus the maximum strain that the gauge read during a displacement step. All points from a given displacement step are connected with a dashed line due to the uncertainty in strain between points. The strain, as a function of distance above the top of the footing, exponentially increases up to a height of 15 inches above the top of the footing. At 15 inches above the top of the footing there is a discontinuity in the strain profiles. The post-installed headed bars extended to 15 inches above the top of the footing and are the reason for the discontinuity in the CFRP wrap strain profiles. The mechanisms that transfer tension to the CFRP wrap are the headed rebar and the column bearing on the non-shrink concrete. The discontinuity in the strain profile signifies the contribution that the headed rebar plays in transferring tension to the CFRP wrap.

The performance of the headed rebar used for the repaired specimen NM-R is studied in this section. The six No. 8 headed rebar provided sufficient flexural strength and tension transfer between the column and footing to successfully relocate the plastic hinge region to the top of the repair. Two strain gauges were placed halfway up the free length of the headed rebar, correlating to 7.5 inches above the top of the footing, on the extreme east and west headed bars prior to testing. The data recorded during testing from these strain gauges are shown in Figure 4.17. The strain gauge on the east headed rebar went off scale during the 2-in. displacement step due to the high level of strain that the bar experienced.

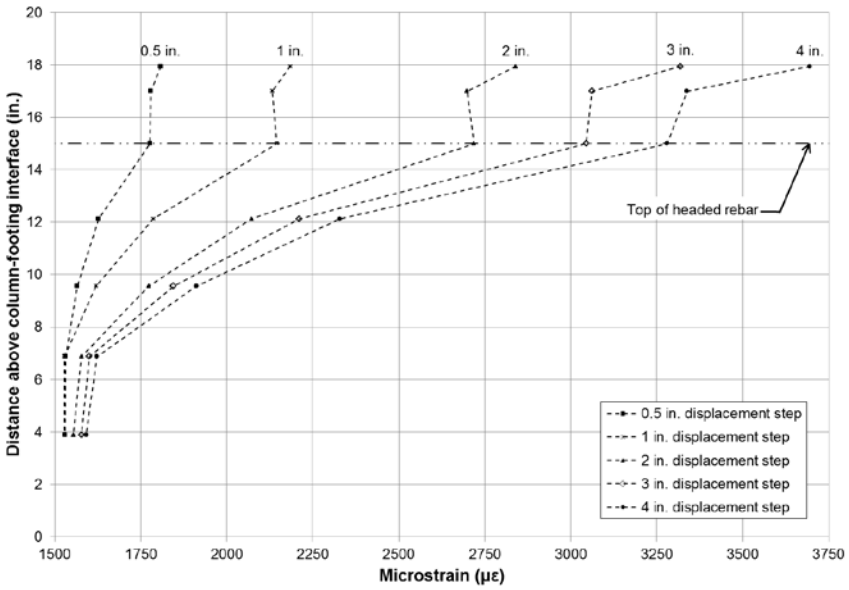

Figure 4.16 NM-R west face wrap strain profile up to 4-in. displacement step

The behavior of the headed rebar observed during testing seems to be influenced by the final damage state. The east longitudinal rebar in the column of NM-R fractured during testing, diminishing the flexural capacity of the specimen in that direction. The headed rebar replaced this lack of flexural capacity in both tension and compression, creating a bending moment couple. The east headed rebar yielded in tension during the 1-in. displacement step, reaching strains of over 1.9 times the yield strain during this displacement step. After the 1-in. displacement step the east strain gauge was lost. It is assumed that the east headed bar went well beyond 1.9 times the yield strain in subsequent displacement steps. The west headed rebar yielded in compression during the 3-in. displacement step, reaching compressive strains of nearly 2.8 times the yield strain during the 7-in. displacement step.

Plastic hinge relocation of NM-O was successfully achieved by NM-R, as shown in Figure 4.17. The hysteretic response of the repaired specimen NM-R is compared in Figure 4.18 with the hysteretic response of the as-built specimen NM-O superimposed. It can be seen that the repaired specimen had an approximately 30% larger lateral load capacity than the as-built specimen. This increase in load capacity is thought to be due to two reasons. First, the moment arm for the repair test is decreased by nearly 20% due to the height of the repair; therefore, a larger load is required to achieve a plastic hinge. Second, the repair test occurred after the as-built test; therefore, the concrete compressive strength of the as-built concrete was larger.

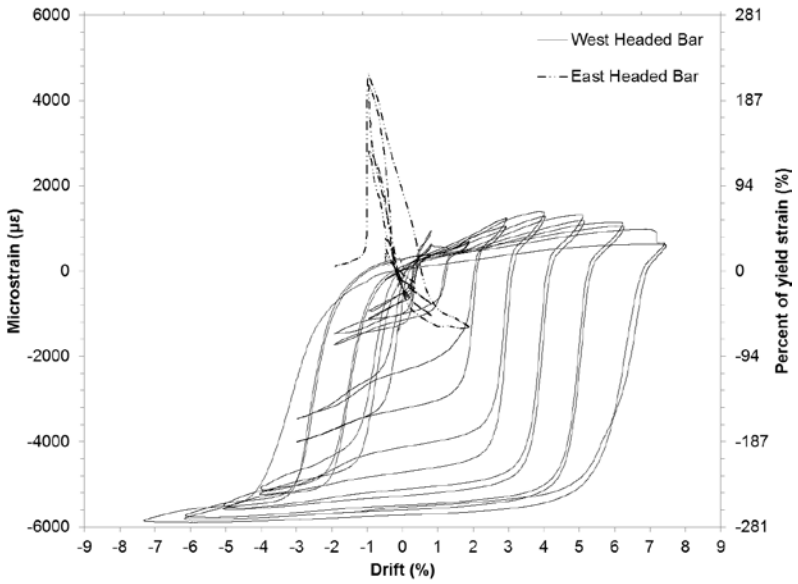

Figure 4.17 NM-R headed bar strain gauge data from 7.5 inches above the footing level

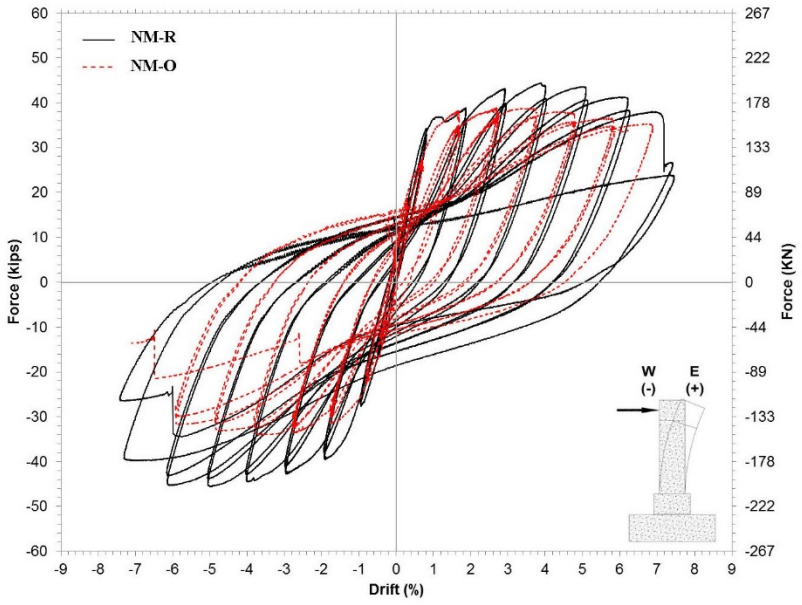

Figure 4.18 Comparison of hysteresis curves for NM-O and NM-R

The displacement capacity of NM-R is slightly greater than the displacement capacity of NM-O. This is an interesting outcome because the repair should have a decreased displacement capacity due to the shortened column length. The shortened column means that for a given displacement, the repair would have a larger rotational demand than the as-built one. However, the as-built joint is a connection of precast concrete elements using GGSS connectors, and the displacement capacity may be adversely affected due to slip and rocking. The repair transforms the precast joint into a system that performs more like a monolithic assembly. The averaged displacement ductility of NM-R of 5.95 is nearly identical to the displacement ductility of NM-O of 6.10. The repair was capable of restoring the diminished load,

displacement, and displacement ductility capacity of the precast joint, which had experienced severe damage.

The hysteretic energy dissipation and stiffness degradation characteristics were investigated and compared to NM-O, as seen in Figure 4.19(a) and Figure 4.19(b), respectively. The cumulative energy dissipation of NM-R is slightly greater than NM-O for all drift ratios; at the completion of the 6% drift ratio, NM-R has dissipated 15% more energy than NM-O. The stiffness degradation characteristics of NM-R and NM-O are very similar when normalized to the 0.5% drift ratio stiffness. The normalized stiffness of NM-R is slightly larger than NM-O at all drift ratios. These performance parameters confirm that the repair restored the assembly to a performance level similar to the original condition. Further details of the repair method for column-to-footing joints are presented elsewhere [18].

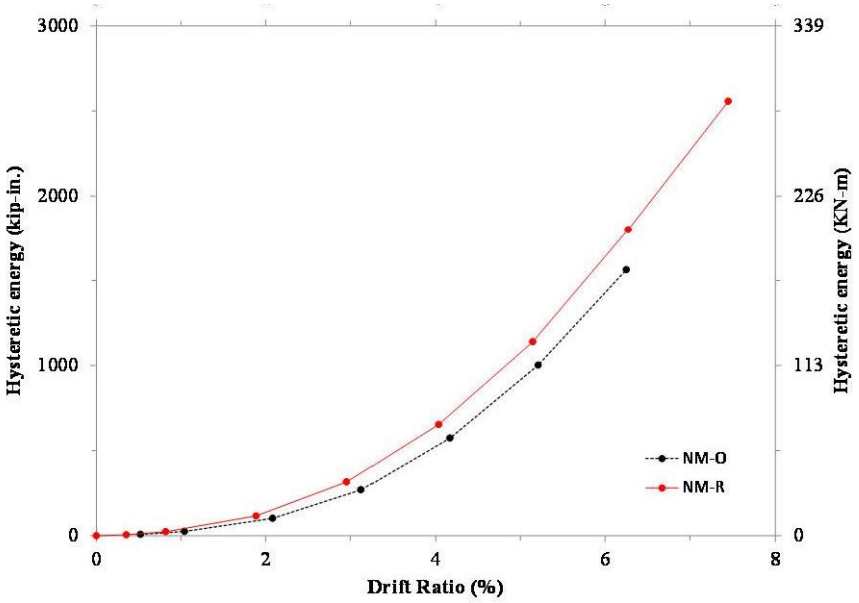

(a)

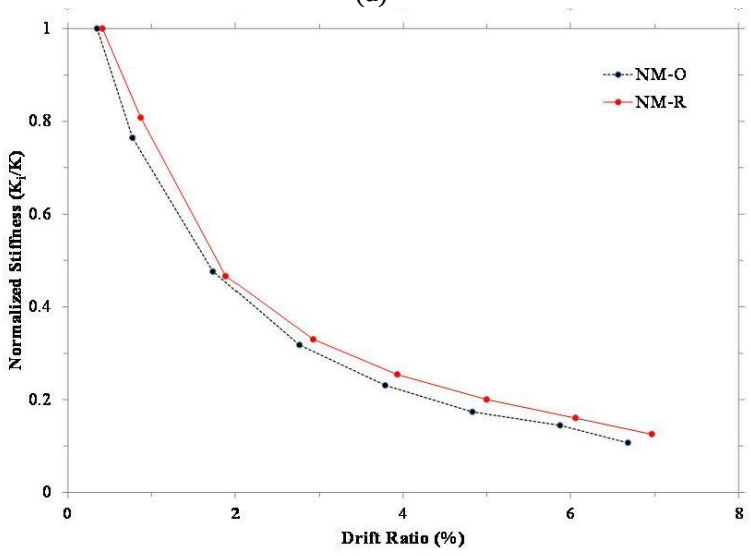

(b)

Figure 4.19 NM-R performance comparison: (a) hysteretic energy dissipation, (b) normalized stiffness degradation

4.3.2 Repaired Column-to-pier cap Joint LE-R – Static Pushover

A static pushover test was applied to specimen LE-R before the cyclic quasi-static test was carried out. The static pushover consisted of a displacement to the east equal to 6.65 in. The column at this maximum displacement is shown in Figure 4.20. It can be seen that the plastic hinge has been successfully moved above the repair with extensive spalling on the east side of the column that extends up to 20 inches from the top of the repaired section. There are, in addition, major flexural cracks that opened on the west side of the column at 2 inches, 9 inches, and 12 inches above the repaired section.

After the monotonic pushover, LE-R was pulled back to zero displacement and the damage was assessed. Figure 4.21 shows the damage to the column with the loose concrete removed and the column at zero displacement. Cracks observed from the test of the as-built specimen LE-O are marked in red, while the cracks that occurred from the pushover test of the repaired specimen LE-R are marked in black. With the cracks closed, it can be seen that the cracks observed during the monotonic pushover at 2 inches and 12 inches above the repaired section were existing cracks that opened up, while the crack that was observed at 9 inches above the repaired section is new. From the test observations of LE-O, the existing cracks at 2 and 12 inches were originally hairline cracks, but after the monotonic pushover, they had grown substantially to a width of 0.05 inches. The new crack that opened at 9 inches had a width of 0.016 inches. With all the loose concrete removed from the east side of the column, it can be seen that the concrete cover had been crushed, thus exposing the spiral reinforcement. Also, there were four radial cracks in the new non-shrink concrete added for the repair. These cracks extended from four corners of the column out to the CFRP jacket and had a width of 0.01 in.

The monotonic pushover curve shown in Figure 4.22 was obtained during the static push test. Point A in the figure corresponds to the maximum lateral load from the monotonic pushover, which occurred at a drift level of 2.97%. After the maximum lateral load was reached, the concrete on the east side of the column began to crush and the lateral load began to decrease until the actuator was stopped at point B. To determine the displacement ductility of LE-R from the monotonic pushover curve, an idealized elastoplastic curve is superimposed on the monotonic pushover curve. Point C represents the theoretical yield point of the system. To obtain the elastoplastic curve, the equal area method was used. The displacement ductility was computed by dividing the drift at point B by the drift at point C; a ductility of 6.6 was obtained for LE-R from the monotonic pushover. The results for LE-R are from a monotonic pushover instead of a cyclic test and cannot be reasonably compared to the results of LE-O, but the value of 6.6 is believed to be slightly above the ductility of the specimen under cyclic loads.

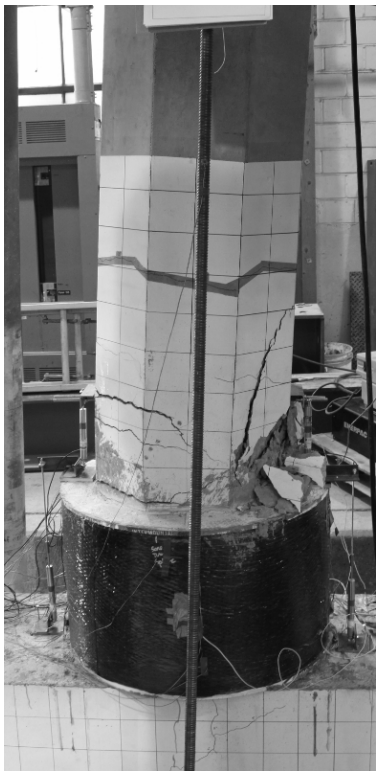

Figure 4.20 Specimen LE-R monotonic pushover at maximum drift

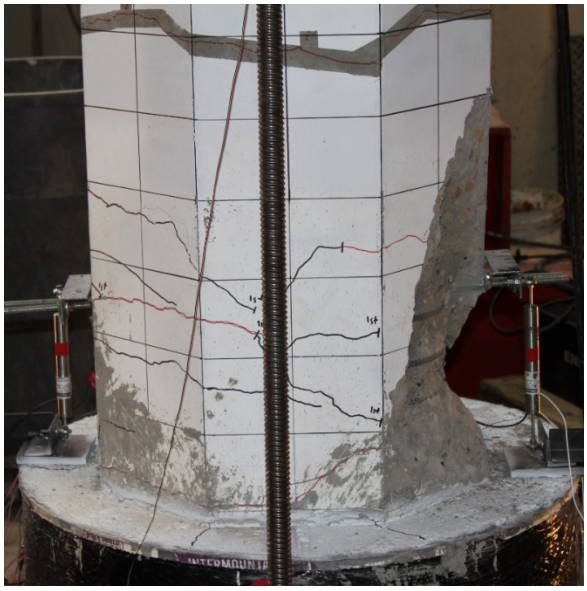

Figure 4.21 Specimen LE-R monotonic pushover damage

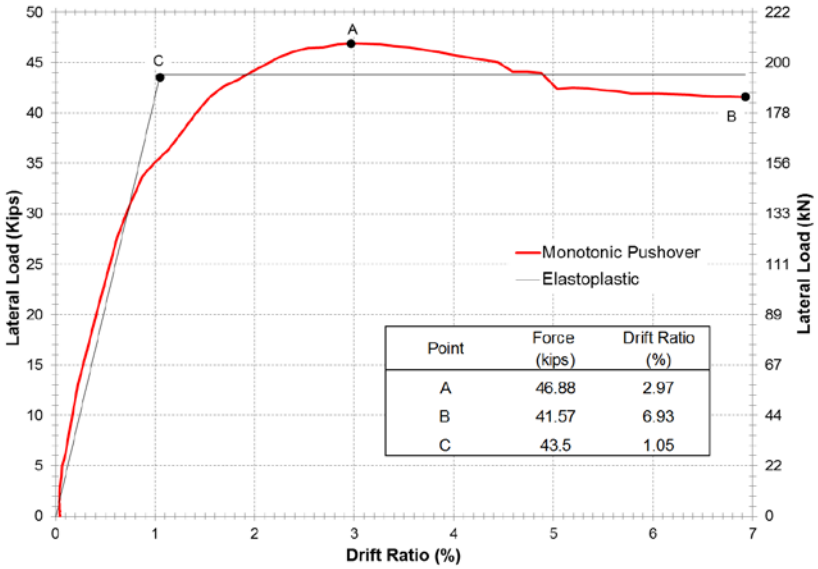

Figure 4.22 LE-R monotonic pushover curve

To better understand the behavior of LE-R during the monotonic pushover, an analysis of the moment versus curvature of the repaired region and the region of the column just above the repair was performed using experimental data. Figure 4.23 shows the moment curvature of these two sections; it is clear that the stiffness of the repaired region was much greater than that of the original column. Also, once the maximum moment was reached, the repaired section experienced no additional curvature since larger deformations took place in the column just above the repair. In addition, pier cap deflection and slippage of the test specimen were negligible.

The strains that were observed in the CFRP jacket during the monotonic pushover were examined. Figure 4.24 shows the hoop strain on the east side of CFRP jacket which is the direction that the column was pushed. Strain gauges 1E, 2E, 3E, and 4E were located 2 in., 4 in., 9 in., and 14 in. below the top of the CFRP jacket, respectively This side of the jacket experienced the highest strain; the amount of strain decreases towards the pier cap. Figure 4.24 shows a noticeable plateau in the CFRP jacket hoop strain; this occurs at about the 3% drift level which is where the maximum horizontal load occurred. The fact that the strains in the jacket remain constant after the maximum lateral load is reached suggests that the strains in the CFRP jacket are more dependent on the applied horizontal load rather than the displacement of the column.

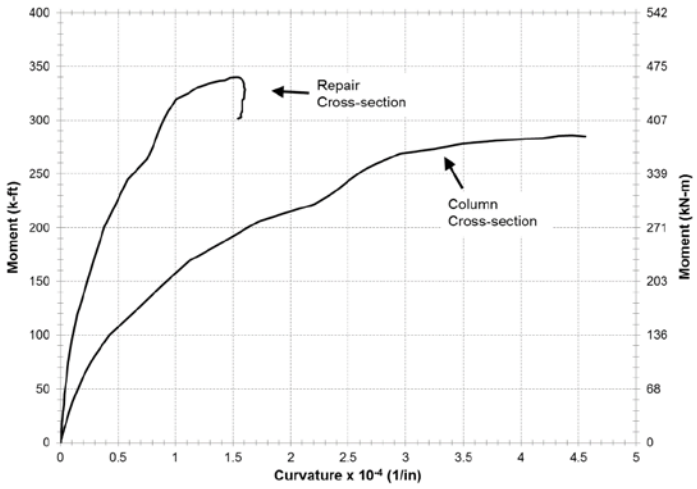

Figure 4.23 LE-R monotonic pushover moment-curvature

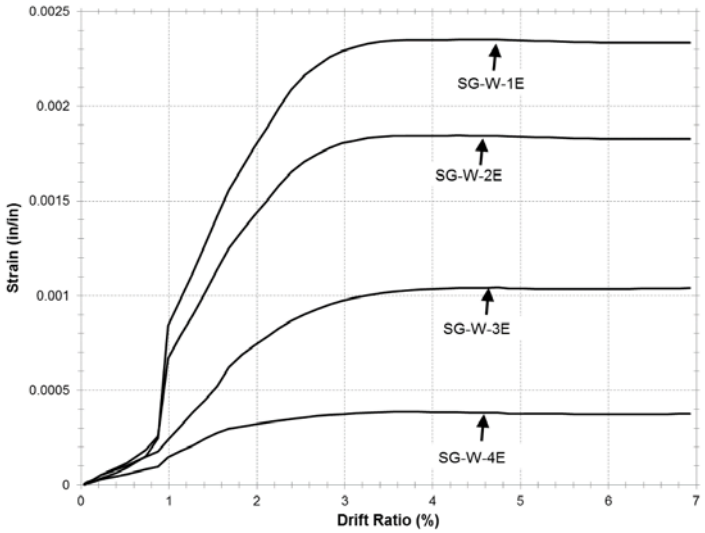

Figure 4.24 LE-R east CFRP jacket hoop strains

Strains in the extreme headed bars during the monotonic pushover test are presented in Figure 4.25. Since the column was pushed to the east, Figure 4.25 shows that the post-installed headed bars on the west side of the column pick up the tension and transfer it to the pier cap while the east headed bars go into compression. From these strain gage data, it is clear that none of the instrumented post-installed bars have exceeded the yield strain of 0.00207 in./in.

The headed bars also have a plateau or drop in strain near the drift level at which the maximum lateral load occurred. Similar to the strain in the CFRP jacket, the strain in the headed bars depends more on the horizontal load rather than the column displacement.

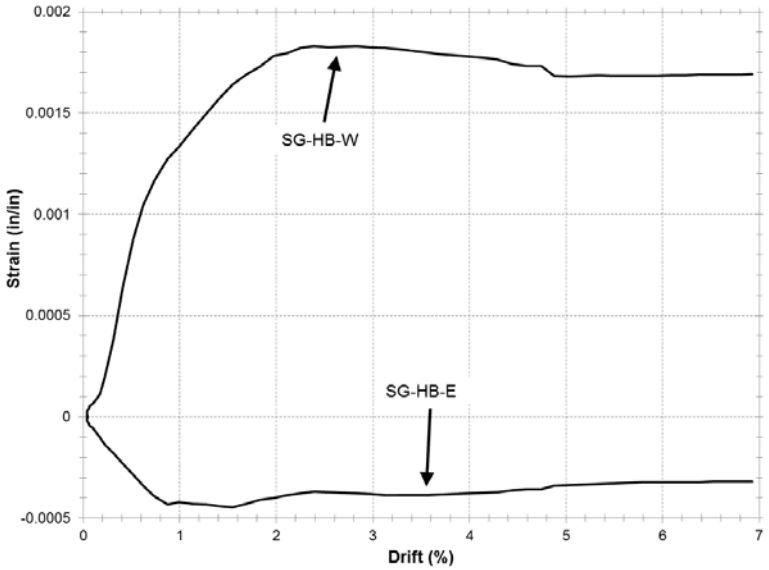

Figure 4.25 LE-R headed bar strains

4.3.3 Repaired Column-to-pier cap Joint LE-R – Cyclic Test

Repaired specimen LE-R, which was already damaged from the monotonic pushover test, was retested using the loading protocol shown in Figure 2.7. Even with the initial damage from the monotonic pushover, the column was able to reach a maximum drift of 7.2% and a maximum lateral load of 40.5 kip before fracturing the extreme east longitudinal column bar just above the repaired section. To clearly see the relocation of the plastic hinge in LE-R, Figure 4.26 compares specimens LE-O and LE-R at maximum drift. In Figure 4.26(a), the plastic hinge formed just above the pier cap while in Figure 4.26(b), the plastic hinge was relocated to a position just above the repair. Figure 4.27 shows the final damage of the west side and east side of the column. The west face of the column had spalling that went 10 inches up the face of the column, exposing transverse reinforcement. On the east column face, additional spalling of the concrete occurred, exposing more of the column reinforcement; ultimately the extreme longitudinal bar on this side fractured. No additional flexural cracks developed during the test. The cracks that developed from the monotonic pushover test just continued to widen from 0.05 to 0.125 inches by the end of the cyclic test.

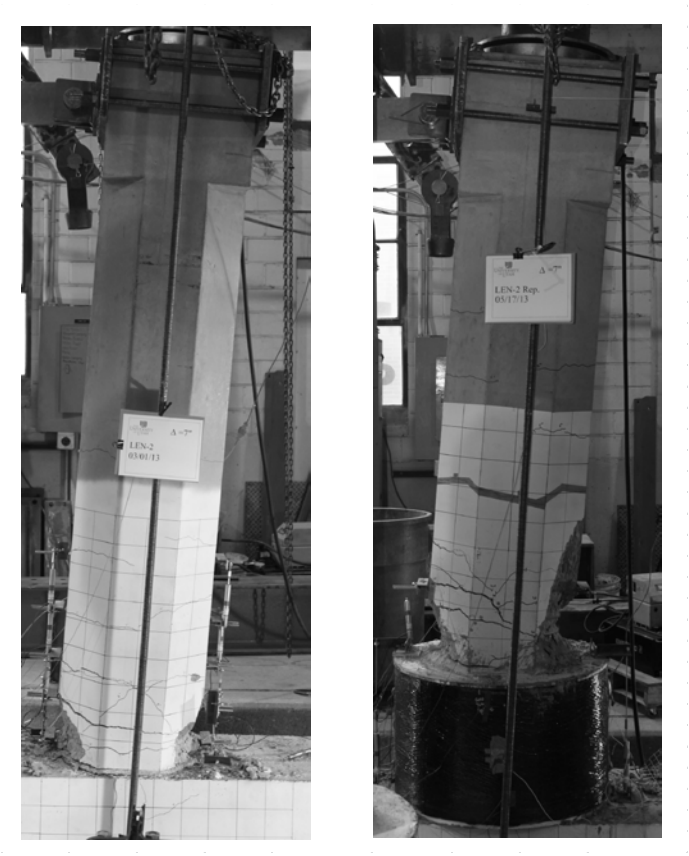

(a) (b)

Figure 4.26 Test Comparison: (a) LE-O at maximum drift, (b) LE-R at maximum drift

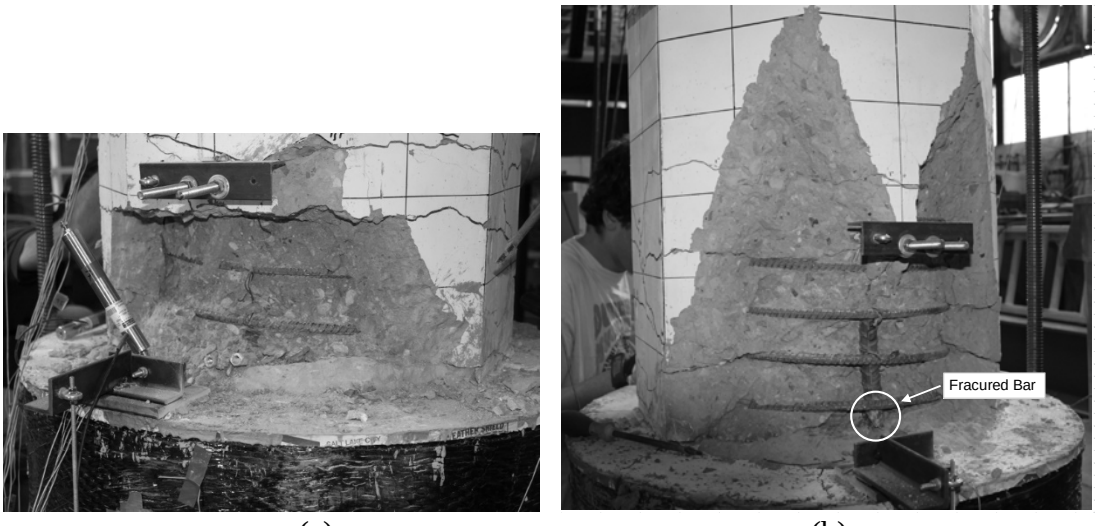

(a) (b)

Figure 4.27 Final damage of repaired specimen LE-R: (a) west face, (b) east face

Figure 4.28 shows the hysteretic response for the cyclic test of repaired specimen LE-R. When the column was pulled back to zero displacement after the monotonic pushover test, it required a lateral force of -22 kip to maintain this position due to the permanent deformation of the steel reinforcement. Therefore, instead of the hysteresis curve beginning at zero force and zero displacement, it begins at a force of -22 kip and zero displacement. Since there was extensive damage to the column from the monotonic pushover test, the right side of the hysteresis curve has an unusual shape. The left side of the hysteresis, however, was only slightly affected from the monotonic pushover test and has a more normal shape since the column had not yet been displaced in that direction.

Two notable observations during the cyclic test are marked on the hysteresis in Figure 4.28. The square symbol marks the cycle in which transverse cracking of the CFRP jacket began to occur and the circle symbol denotes fracture of the column longitudinal reinforcement. Note that there is no apparent change in the hysteresis curve due to the transverse CFRP crack. The cracking of the CFRP jacket occurred just above the top of the headed bars and is shown market by a white line in Figure 4.29. The crack in the CFRP had a final width of 0.125 inches, a length of 38.75 inches, and only existed on the west side of the jacket. The crack was caused by an increased curvature demand on the repaired section when the column was pushed to the west.

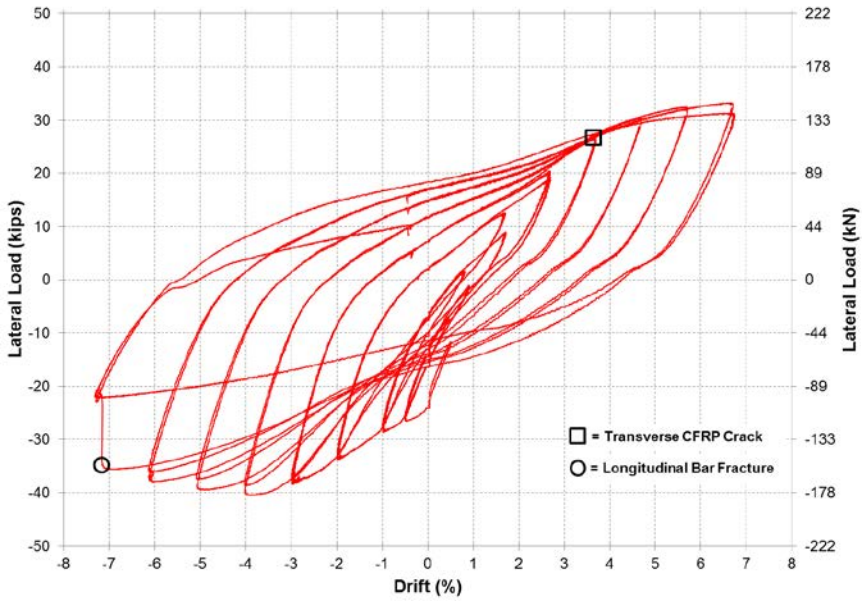

Figure 4.28 Repaired specimen LE-R hysteresis curve

Figure 4.29 LE-R transverse CFRP crack

Figure 4.30 compares both the monotonic pushover and cyclic hysteresis results of repaired specimen LE-R to the as-built specimen LE-O. Since the right side of the hysteresis of LE-R represents a column that was severely damaged from the monotonic pushover test, it was ignored for the comparison. From Figure 4.30 it can be seen that the lateral load for both the monotonic pushover and cyclic tests of LE-R is larger than the lateral load for LE-O. This increase in the lateral load was expected since moving the plastic hinge up the column shortens the moment arm to that section. The displacement capacity of LE-R is the same as that of LE-O for both the monotonic pushover and cyclic tests. Since there was no test of LE-R that can be directly related to LE-O, it is difficult to make an absolute comparison in terms of displacement capacity, ductility, and energy dissipation. However, from the results observed, it would be appropriate to conclude that LE-R would have performed at least as well as LE-O if it were tested under identical conditions.

Also in Figure 4.30, a mirrored plot of the monotonic pushover is superimposed in the 3rd quadrant of the graph in order to compare the monotonic pushover performance to the cyclic performance of LE-R. From this comparison, it can be seen that up to a drift level of -3% the hysteretic response of LE-R was slightly affected by the initial damage from the monotonic pushover. After a drift level of -3%, however, the hysteretic response of LE-R does not appear to be affected by the initial damage from the monotonic pushover and follows a similar shape to the monotonic pushover curve. Further details of the repair method for column-to-pier cap joints are presented elsewhere [19].

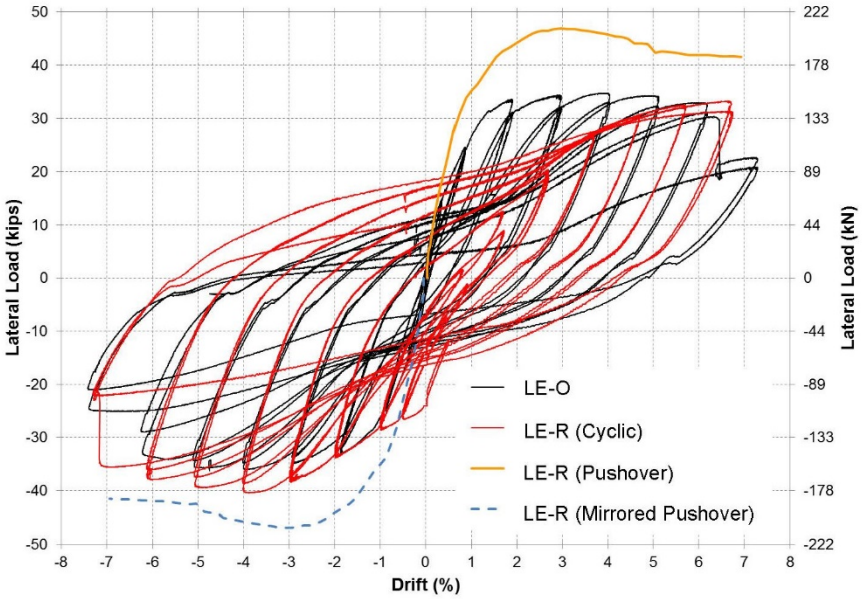

Figure 4.30 Comparison of test results for as-built specimen LE-O and repaired specimen LE-R

4.3.4 Comparative Study of As-Built and Repaired Joints

Table 4.2 shows a comparison of all the tests. In all cases, the repaired specimens were able to regain the strength of the original specimens while still performing in a ductile manner. For the case of NM-R, a 15% increase in the maximum lateral load was obtained while still maintaining the ultimate drift ratio capacity and displacement ductility. For the case of LE-R, it is difficult to make direct comparisons to LE-O, because of the initial static pushover test. However, by examining the performance of LE-R from both the static pushover and cyclic tests, it is clear that it performed at least as well as LE-O.

Table 4.2 Comparison of test results

Test Criteria	NM-O	NM-R	LE-O	LE-R (Pushover)	LE-R (Cyclic)
Max Lateral Load (kips)	38.8	44.6	37.7	46.8	40.5
Ultimate Drift Ratio (%)	6.42	6.96	6.50	6.88	7.2
Displacement Ductility	6.1	6.0	5.9	6.6	---
Failure Mode	Bar Fracture	Bar Fracture	Bar Fracture	---	Bar Fracture

5. CONCLUSIONS

5.1 Summary

A rapid procedure tailored to repair earthquake damaged bridges has been developed. The repair method concerns severely damaged bridge joints connected using Grouted Spliced Sleeve connectors. The damage state of the specimens prior to the repair was severe, including longitudinal rebar buckling and fracture in the columns of the column-to-footing joints, and longitudinal rebar fracture and bar pullout in the columns of the column-to-pier cap joints. The repair method converts the original plastic hinge region from a 21-in. octagonal cross section to a 30-in. diameter circular section for a column height equal to 18 inches, thereby relocating the new plastic hinge. The repaired region extends up the column height for a length sufficiently long enough to cover the original plastic hinge region and is reinforced with headed bars and a CFRP shell. This repair procedure was implemented and tested for previously damaged bridge column-to-footing and column-to-pier cap joints; it successfully restored the diminished performance of the specimens in terms of displacement capacity, load capacity, energy dissipation, and stiffness. The repair method is a rapid technique for seismic repair or retrofit of precast columns in column-to-footing or column-to-pier cap connections.

5.2 Findings

The design and implementation of the repair method outlined in this report successfully relocated the plastic hinge region of the specimens. Throughout the research process, a few design improvements were recognized and should be considered for future applications.

The thickness of the CFRP wrap should be larger than that calculated in Section 4.1 by an appropriate margin of safety. This is necessary because the tensile strength of steel reinforcement and concrete compressive strength of the as-built structure might be underestimated. The shear strength and confinement the CFRP wrap provides is paramount to the good performance of the repaired region. To ensure good performance from the CFRP wrap, all available methods to mitigate transverse CFRP cracking should be taken. This includes decreasing the cover of the headed rebar. Additional means of providing longitudinal strength to the CFRP wrap should also be investigated.

The experiments carried out in the present research provided qualitative and quantitative measures for the performance of each individual subassembly. The repair method explored in this research was successful; it provides an attractive alternative to the high cost and user interruption that bridge replacement poses after a large earthquake. The repair procedure is rapid, cost effective, corrosion resistant, easily constructible, and uses readily available materials. Future applications of the repair method may be expanded to all types of column plastic hinges in bridges for precast or monolithic construction. However, necessary shear reinforcement is required to achieve satisfactory performance. In columns of existing bridges that lack the shear reinforcement required for the repair method, the use of externally bonded shear reinforcement should be implemented.

6. REFERENCES

[1] M.J. Ameli. “Seismic Design of Grouted Splice Sleeve Connections for Bridge Piers used in Accelerated Bridge Construction,” Ph.D. Dissertation, University of Utah, Salt Lake City, UT, 2015.

[2] Z. Haber, M. Saiidi, and D. Sanders. “*Precast Column-Footing Connections for Accelerated Bridge Construction in Seismic Zones,”* Final Report No. CA13-2290, Nevada, 2013.

[3] A. Belleri, and P. Riva. “Seismic Performance and Retrofit of Precast Concrete Grouted Sleeve Connections,” *PCI Journal*, vol. 57, 97–109, 2012.

[4] F. Seible, M.J.N. Priestley, and G. Hegemier. “Seismic Retrofit of RC Columns with Continuous Carbon Fiber Jackets,” *Journal of Composites for Construction*, vol. 1, 52–62, 1997.

[5] C.P. Pantelides, I. Gergely, L.D. Reaveley, L.D., and V.A. Volnyy. “Retrofit of R/C Bridge Pier with CFRP Advanced Composites,” *Journal of Structural Engineering*, vol. 125, 1094–1099, 1999.

[6] Y. Chai, M.J.N. Priestley, and F. Seible. “Seismic Retrofit of Circular Bridge Columns for Enhanced Flexural Performance,” *ACI Structural Journal*, vol. 88, 572–584, 1991.

[7] D. Lehman, S. Gookin, A. Nacamuli, A., and J. Moehle. “Repair of Earthquake-Damaged Bridge Columns,” *ACI Structural Journal*., vol. 98, 233–242, 2001.

[8] Y.D. Hose, F. Seible, and M.J.N. Priestley. “Strategic Relocation of Plastic Hinges in Bridge Columns,” Final Report SSPR 97–05, University of California, San Diego, CA, 1997.

[9] S. Rutledge, M. Kowalsky, R. Seracino, and N. Nau. “Repair of Damaged Circular Reinforced Concrete Columns by Plastic Hinge Relocation,” Proceedings of the 15 WCEE, Lisbon, 2012.

[10] American Association of State Highway and Transportation Officials (AASHTO). “AASHTO LRFD Bridge Design Specifications.” AASHTO, Washington, DC, 2012.

[11] American Association of State Highway and Transportation Officials (AASHTO). “AASHTO Guide Specifications for LRFD Seismic Bridge Design.” AASHTO, Washington, DC, 2011.

[12] California Department of Transportation. “*Seismic design criteria* - Division of Engineering Services.” Sacramento, CA, 2010.

[13] American Concrete Institute. “ACI 374.2-13 Guide for Testing Reinforced Concrete Structural Elements under Slowly Applied Simulated Seismic Loads.” Farmington Hills, MI, 2013.

[14] American Concrete Institute. “ACI 318-11 Building Code Requirements for Structural Concrete.” Farmington Hills, MI, 2011.

[15] Hilti Corporation. “Technical application document Hilti HIT-RE 500-SD.” Champs sur Marne, France, 2010.

[16] C.P. Pantelides, and D.A. Moran. “Design of FRP jackets for plastic hinge confinement of RC columns,” *Journal of Composites for Construction*, Vol. 17, 881–898, 2013.

[17] American Concrete Institute. “ACI 440.2R-08 Guide for the Design and Construction of Externally Bonded FRP Systems for Strengthening Concrete Structures.” Farmington Hills, MI, 2008.

[18] D.N. Brown, “Post-earthquake Repair of Precast Concrete Column-to-Footing Plastic Hinges.” M.S. Thesis, University of Utah, Salt Lake City, UT, 2014.

[19] J.E. Parks, “Seismic Rehabilitation of Column to Pier Cap Accelerated Bridge Construction Connections and Acoustic Emission Monitoring Assessment.” M.S. Thesis, University of Utah, Salt Lake City, UT, 2014.